Multiphase Flow in Porous Media with Emphasis on CO_2 Sequestration

Alif Be

Dissertation for the degree philosophiae doctor (PhD)

at the University of Bergen

2011

Alif Be

Centre for Integrated Petroleum Research

Department of Physics and Technology

University of Bergen

Allegaten 41

N-5007 Bergen

Norway

Preface

This dissertation was submitted for the degree Philosopiae Doctor at the University of Bergen. The dissertation consists of three papers, two internal reports and an introduction including theoretical background. The papers and internal reports are based work done in the period 2007 to 2011 at the Centre for Integrated Petroleum Research at the University of Bergen.

The subject of this thesis is multiphase flow in porous media with emphasis on CO_2 sequestration. The impact on wettability alteration on CO_2 storage safety is studied for both Johansen formation and synthetic model. Different mechanisms that enhance or prevent CO_2 leakage are analyzed in relation with wettability alteration.

In addition, the impact of three-phase capillary pressure for three different sets of wettability in three-phase flow is evaluated. Three-phase capillary surfaces were generated from network modelling.

Acknowledgements

I would like to express my gratitude to my supervisors Professor Arne Skauge for giving me the opportunity to undertake this study and for excellent academic and professional guidance, advice, and support throughout the course of this work. I have learned so much during this period.

I also would like to thank Dr. Alex Larsen for introducing me to this great PhD program and his support throughout my PhD study. Thanks to my colleagues at Perecon AS and Weatherford Petroleum Consultant AS for giving me flexibility so that I can work on my thesis.

I wish to acknowledge Norwegian Research Council (NFR) for financial support during this work. Thanks to my fellow students and colleagues at the CIPR particularly in the administration section to provide a social environment and a friendly workplace. Special thanks to Saeed Fallah for good discussion and being great room-mate.

Finally, but not least, I would like to thank my dearest Yan Dong for putting up with me during this work by encouragement and unconditional support. I am truly grateful.

7nd October 2011

Alif Be

List of publications

1. Be, A., (2011): “Including Three-phase Capillary Pressure Flow Description into UTCHEM”, Internal Report, CIPR

2. Be, A., (2011): “Application of Experimental Design and Ensemble Kalman filter for Capillary Pressure Matching”, Internal Report, CIPR

3. Be, A., Skauge, A., Delshad, M. (2011): “Simulation of Three-phase Flow in Porous Media Including Capillary Pressure Representing Variation in Rock Wettability”, paper for the 16th European Symposium on Improved Oil Recovery, Cambridge, United Kingdom, 12-14 April 2011.

4. Be, A., Kolstø, S., Skauge, A., (2011): “Sensitivity Study of Cap Rock Integrity on CO_2 Storage”, submitted to International Journal of Greenhouse Gas Control

5. Be, A., Skauge, A., (2011): “Wettability Alteration Effect to CO_2 Sequestration Flow Mechanism”, in preparation

Contents

1. Introduction

Numerical simulation has been used to predict multiphase flow in porous media. It is of great importance to incorporate accurate flow properties to obtain a proper simulation result thus reducing the risk of making wrong decision.

Relative permeability and capillary pressure are important key parameters in multiphase flow as they describe how different fluid will interact in porous media. It is even more important in the case of three-phase flow as there are more fluid phases interact in the system.

In most of the three-phase flow studies, capillary pressure has been neglected due to the lack of measured data and assumption that its effect is negligible. In other cases, two-phase capillary pressure has been used instead to describe the process in the system. This study will try to show how significant the impact of three-phase capillary pressure using different rock wettability. The three-phase capillary pressure surfaces are generated using a network model.

Prior research shows that rock wettability is altered during CO_2 sequestration due to the formation of carbonic acid (H_2CO_3) which leads to lower pH. In this study the effect of wettability alteration is incorporated to assess the safety of Johansen formation which is a good candidate for CO_2 sequestration project. In addition, the wettability alteration effect to different flow parameters such as heterogeneity, solubility and diffusion is investigated.

This thesis consists of two parts; the first part presents a theoretical background for the work, and the second part is a collection of papers. The papers are grouped into two main topics. The first three papers are discussing about three-phase flow simulation in porous media. The rest are discussing about wettability alteration during CO_2 sequestration.

Chapter 2 and 3 of the theoretical background include definitions and descriptions of interfacial tension, wettability, capillary pressure, relative permeability and hysteresis. Network model and technique for capillary pressure matching are described briefly in chapter 4. Three-phase relative permeability and three-phase capillary pressure are covered in chapter 5. Chapter 6 provides physical and chemical properties of CO_2 with their implication in CO_2 sequestration described in chapter 7. Summary of main results is given in chapter 8. Further work is discussed in chapter 9.

Three papers and two internal reports are included. The titles of the papers are “Simulation of three-phase flow in porous media including capillary pressure for different wettability system”, “Sensitivity study of cap rock integrity on CO_2 storage” and “Wettability alteration effect to CO_2 sequestration flow mechanism”. In addition two CIPR internal reports are included. The titles of the reports are “Application of experimental design and ensemble-Kalman filter for capillary pressure matching” and “Including three-phase capillary pressure flow description into UTCHEM”

2. Interfacial tension and Wettability

Interfacial tension and wettability are key parameters which affect petrophysical properties of reservoir rocks and fluid interaction. Knowledge of these parameters are useful to estimate oil reserve and for prediction of production performance. They affect the distribution of water, oil and gas within reservoir rock, which in turn, affect the displacement behavior and relative permeability characteristics (Mungan (1964), Bardon and Longeron (1980), Kumar et al. (1985), Shen et al. (2006), Abdalllah et al. (2011)) Both Kumar et al. (1985) and Shen et al. (2006) stated that residual oil saturation and relative permeability are significantly altered with changes in IFT for low IFT system. The impact are less significant for high IFT system.

In this thesis, we will investigate the effect of these two parameters on CO_2 storage capacity and three-phase flow in porous media.

As will be discussed in chapter 7, paper 2 and paper 3, CO_2 injection into aquifer will alter both interfacial tension and wettability. Hence it will reduce the capacity of aquifer to keep CO_2 in immobile condition. However, it will also be shown that wettability alteration will reduce mobility of gas, preventing gas to migrate from storage. Thus the overall impacts of these parameters in CO_2 storage capacity should be inspected in detail using reservoir simulation.

These two parameters also have impact on three-phase capillary pressure. Paper 1 present the impact of three-phase capillary pressure with different wettability using our modified version of UTCHEM simulator.

2.1 Interfacial tension

Interfacial tension is a measurement of the cohesive energy present at an interface between two immiscible fluids like oil/water, oil/gas, gas/water. If the fluids are a gas and a liquid the forces acting on the interface is called surface tension. The interfacial

or surface tension is usually denoted using the symbol σ. The surface tension between oil and water, σ_{ow} , is shown in figure 2.1.

The Young-Dupre equation follows from the force balance and is given by

$$\sigma_{os} - \sigma_{ws} = \sigma_{ow} \cos\theta_{ow} \qquad (1)$$

where σ_{os} is the interfacial tension between the oil and the solid , σ_{ws} is the interfacial tension between the water and the solid, and θ_{ow} is the angle between the oil-water interface and the solid.

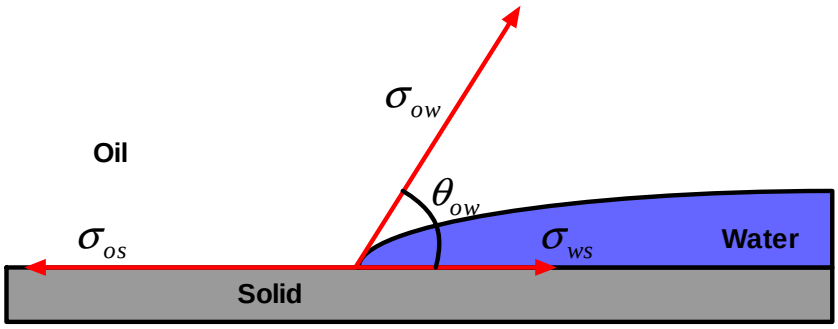

Figure 2.1: Force balance of oil-water-solid

Interfacial tension is obviously very dependent with combination of fluids involved. In addition, experiments results shows that interfacial tension is strongly related to its pressure, temperature, salinity and pH condition.

Okasha and Al-Shiwaish (2009) measured interfacial tension of dead oil and brine system at different pressure, temperature and salinity condition. They found that the interfacial tension increases with increasing pressure and decreases with increasing temperature. This observation is similar to previous experiment result performed by McCaffery (1972) using on n-octane and water as illustrated in figure 2.2. Okasha and Al-Shiwaish (2009) also found that the effect of temperature will be more profound in lower salinity condition while pressure will affect interfacial tension more significantly at higher salinity condition as illustrated in figure 2.3.

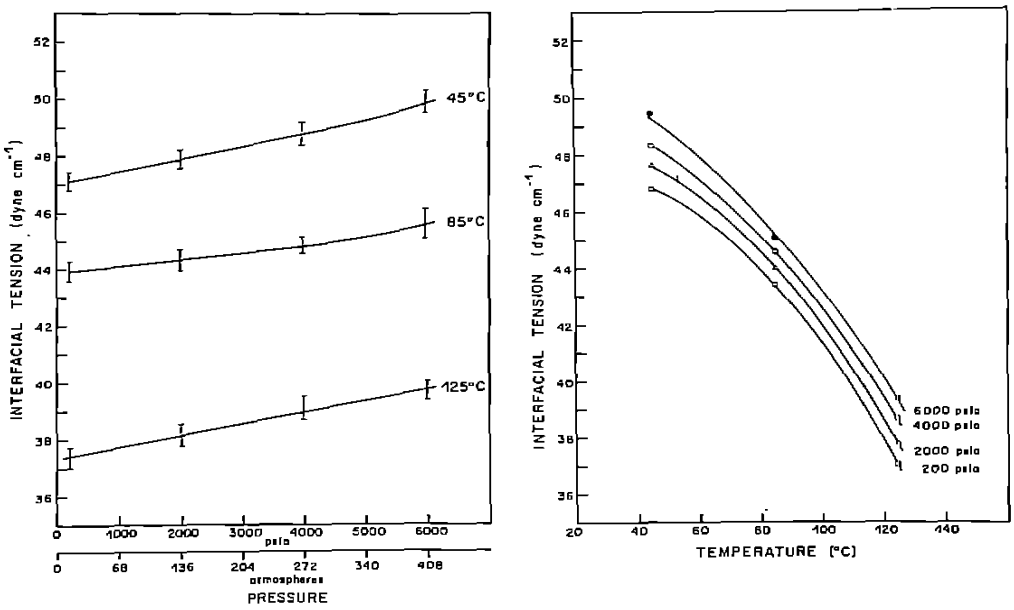

Figure 2.2: Effect of temperature and pressure on n-octane/water interfacial tension. Adapted from McCaffery (1972).

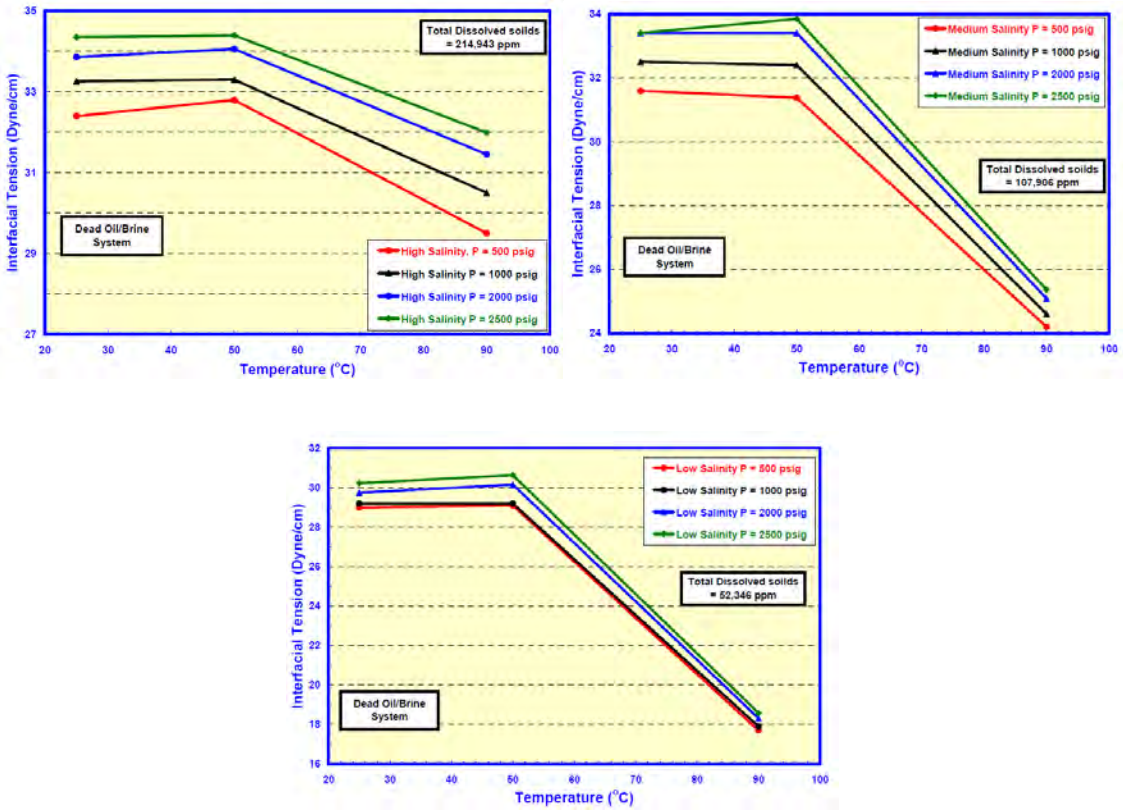

Figure 2.3: Effect of temperature and pressure on interfacial tension for different salinity Arab-D (Carbonate reservoir) dead oil/brine system. Adapted from Okasha and Al-Shiwaish (2009).

Buckley and Fan (2005) measured the effect of pH (in range between 3 and 10) on interfacial tension between crude oil and brine. They grouped their experiment results into two groups based on acid number of the oil and observed that IFT decreases at pH above 7. This observation is in agreement with previously reported by Skauge et al. (1999). In most of the samples, interfacial tension will reach plateau when pH between 5 and 7 except for two samples with low acid numbers.

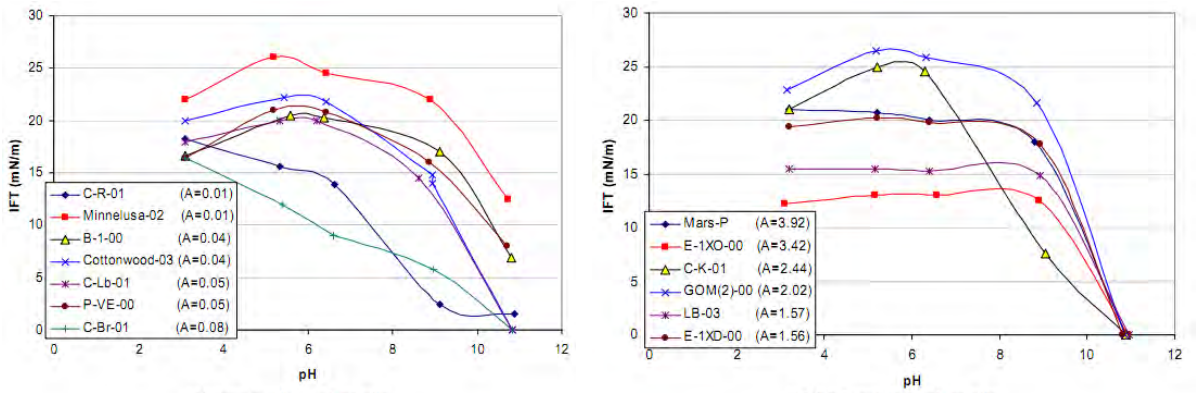

(a) low acid number oils (b) high acid number oils

Figure 2.4: pH dependence of IFT for low and high acid number oils.
Adapted from Buckley and Fan (2005).

Chiquet et al. (2007b) measured interfacial tension for CO_2 and water system and observed that pressure and temperature effect gives a different trend than seen in oil-water system. Their observation indicates that interfacial tension between CO_2 and water decreases with increasing pressure while the effect of temperature on interfacial tension is relatively insignificant. We will discuss their experiment results in more details in chapter 7 when we discuss alteration of key parameters during CO_2 sequestration project.

2.2 Wettability

Wettability is defined as relative degree to which a fluid will spread on a solid surface in the presence of other immiscible fluids. Fundamental understanding of the wettability of rock surfaces by crude oil and brine requires a good description of the

interactions between the different materials in contact. Two mains factors have to be considered. On one side, the morphology of the core: pore size distribution, permeability and porosity; on the other side, the chemical composition and particular interactions between the different phases of oil, brine and rock. Both factors influence the wetting behavior of a particular reservoir and will determine the efficiency of an oil recovery operation by driving fluids, for example, water flooding process.

In the system with more than one fluid, the contact angle between two fluids determines the rock wettability. The contact angle, θ_{ow}, is by convention measured through the denser fluid, in this case the water phase, see figure 2.5. Water-wet rock will have contact angle between 0º to 75º, while gas-wet will have contact angle between 105º to 180º. If contact angle is between these ranges, the rock is considered to have neutral or intermediate wettability.

In the case of neutral wet, due to the fact that the capillary pressure is close to zero, no spontaneous displacement of either fluid by the other will occur. The only way either fluid can be displaced by the other is if an external pressure is imposed on the displacing fluid. No thick films of either fluid exist under conditions of neutral wettability, and it is even possible that the two fluids may flow side-by-side in the same pores.

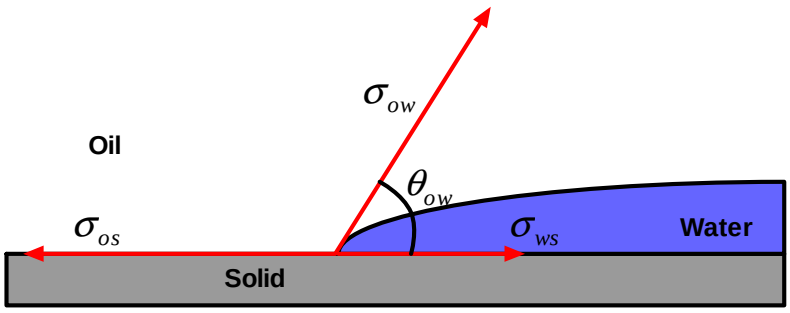

Figure 2.5: Water droplet spreading on a solid surface

In general, there are two types of wettability:

1) Strong wettability

During the evolution of a reservoir or cap rock, most of the rock sediments are deposited in a water environment and the rock is thus initially strongly water-wet.

2) Intermediate wettability

Intermediate wettability describes a condition where there is no dominant phase in terms of wettability. Intermediate wettability is divided into three subclasses: mixed-wet large (MWL), mixed-wet small (MWS) and fractionally-wet (FW). For MWL and MWS, the oil-wet pores are usually the large and small pores respectively. In the case of a fractionally-wet reservoir, the oil-wet and water-wet pores are not distributed with respect to pore size. According to Skauge et al. (2006), fractional wettability could be reflected as spot like oil-wet sites on the surface. This special wettability could be a result of precipitation, variation in mineralogy, or because the pore shape consists of flat surfaces.

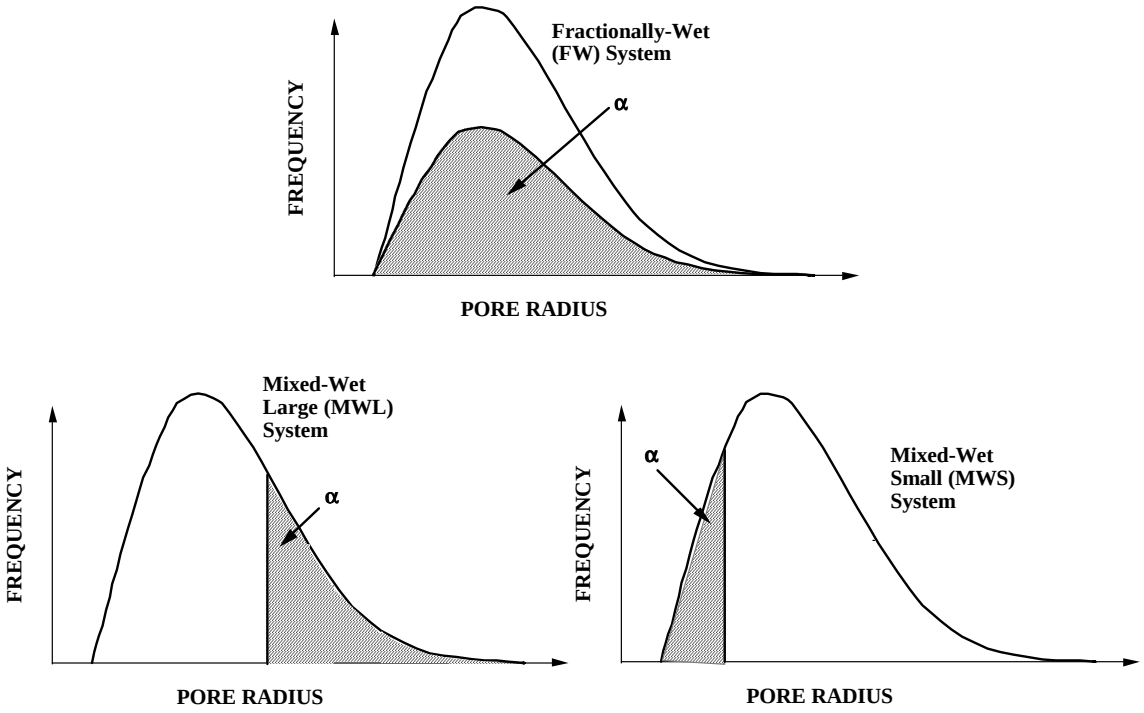

Figure 2.6: Different wettability systems, Adapted from Sorbie and Dijke (2004).

Mixed-wettability rocks are known to have much higher irreducible water saturation compare to uniformly water-wet rocks while uniformly water-wet cores have higher irreducible water saturations than neutral-wet cores (Anderson (1987b)). The higher

irreducible water saturation in mixed-wet cores can be explained by the increased trapping and loss of hydraulic continuity in such a system. On the other hand, Irreducible water saturation decreases with increasing permeability for all wettability classes (Skauge et al. (2006)).

Wettability is very dependent on fluid types, pressure, temperature, and pH. Wang and Gupta (1995) performed experiments on advancing contact angle of two crude oil – brine system for different pressure and temperature. Crude oil (a) is from a carbonate reservoir and crude oil (b) is from a sandstone reservoir. Their experiment results show that contact angle increases with increasing pressure, while the relationship between contact angle and temperature is not straight forward. The two crude oil-brine systems studied shows different trend which indicate the influence of chemical difference between the two systems.

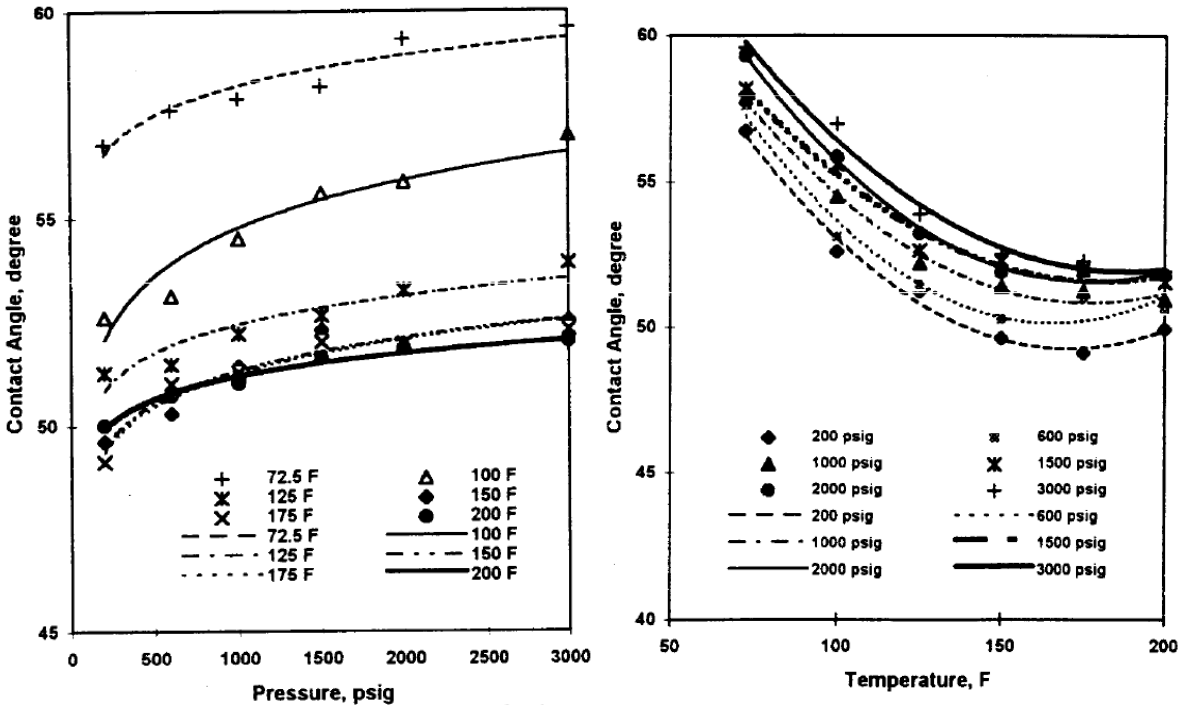

Figure 2.7: Effect of pressure and temperature on contact angle for crude oil-brine(a)-calcite. Adapted from Wang and Gupta (1995).

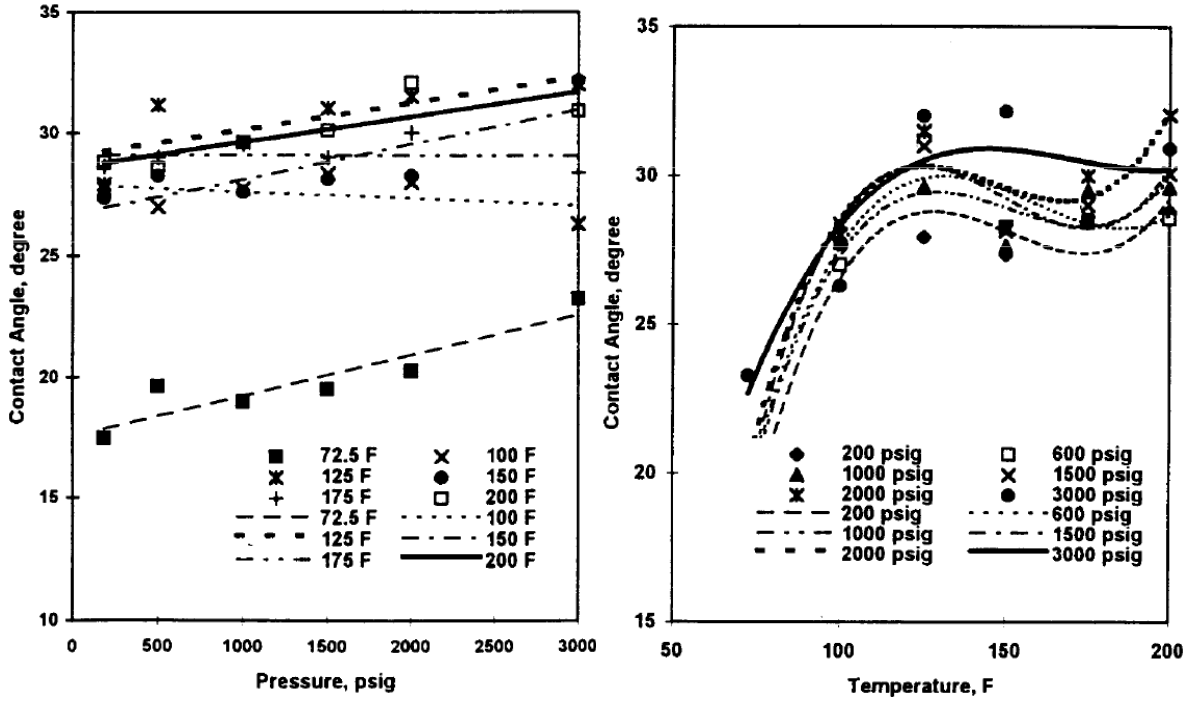

Figure 2.8: Effect of pressure and temperature on contact angle for crude oil-brine(b)-quartz. Adapted from Wang and Gupta (1995).

Skauge et al. (1999) measured contact angle for three crude oils on quartz plate as a function of equilibrium pH. As shown from figure 2.9, contact angle decreases with increasing pH. This trend is related to surface charge of quartz plate which has a point of zero charge at pH 2. At pH higher than 2, quartz surface will be negatively charge hence surface charge of crude oil will transfer into the charges, moving from net positive at low pH values into negative charge at high pH values. As pH is increased, interface between oil-water and water-quartz become more negative, creating repulsive forces which stabilize water film covering quartz surface. This phenomenon is observed as decreasing contact angle behavior of quartz surface.

Several wettability measurements for CO_2-brine on mica and quartz were performed by various researchers (Chiquet et al. (2007a), Shah et al. (2008), Tonnet et al. (2008)). These experiments showed a wettability changes as CO_2 is being in contact with rock. The alteration is a function of CO_2 pressure with weaker water-wet at higher CO_2 pressure. Chiquet et al. (2007a) showed a significant alteration on mica as CO_2 pressure increased, while Tonnet et al. (2008) showed a minor alteration.

However, they agreed on quartz measurements which showed less alteration compared to mica. Their experiment results will be discussed in detail in chapter 7 when we discuss alteration of key parameters during CO_2 sequestration project.

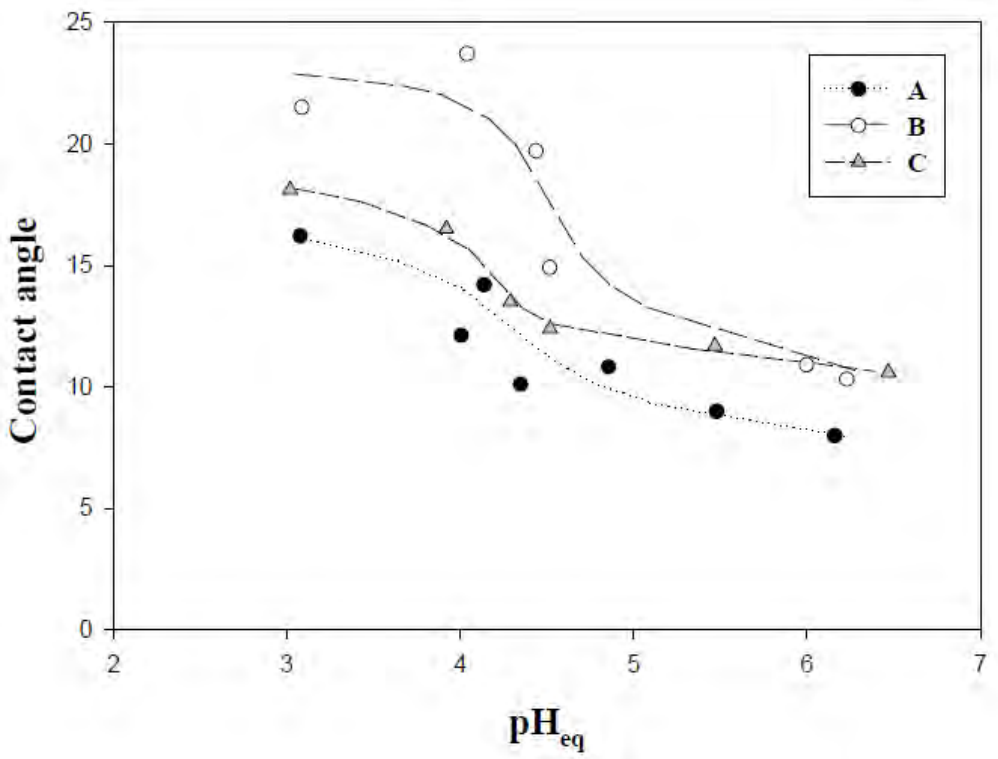

Figure 2.9: Effect of equilibrium pH in the aqueous phase on contact angles for crude oils. Courtesy of Skauge et al. (1999)

3. Multiphase flow in porous media

Flow study in porous media requires good description of rock and fluid properties. Single phase flow is relatively simple to describe since there is not any interaction between fluids. Flow efficiency in such system is dependent on the rock permeability which is independent on type of fluid that flow in it.

Multiphase flow in porous media is a complex process. Proper modelling of multiphase flow required good description of fluid interaction such as capillary pressure and relative permeability. Including these two parameters into reservoir simulation will increase complexity of numerical calculation. In some cases, these two parameters, especially capillary pressure, will create instability in numerical simulation. In this thesis, we have chosen to use analytical model for both parameters since they will give more stable simulation. The reason for this is that analytical model has a smooth curve which has smooth derivation.

This chapter will also discuss hysteresis and trapping models which is especially useful to describe the process in simulation of CO_2 sequestration, as reported in both paper 2 and paper 3.

In this chapter, we will only describe saturation function describe in two-phase flow system. Three-phase flow system will be described in detail in chapter 5 of this thesis.

3.1 Capillary pressure

When two immiscible fluids contact each other in a pore channel, their interface will tend to curve due to the stronger adhesive force of the wetting fluid. The capillary pressure is defined as the molecular pressure difference across the interface of two fluids. The capillary pressure in a circular pore throat is expressed as:

$$P_c = \frac{2\sigma \cos\theta}{r} \tag{5}$$

where σ is the interfacial tension between the phases, θ is the contact angle, and r is the pore throat radius, shown in figure 3.1.

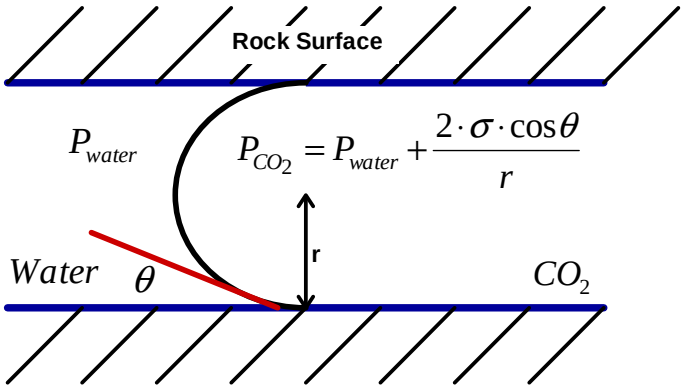

Figure 3.1: Capillary pressure in a circular tube

Capillary pressure is often described as a function of wetting phase saturation as illustrated in figure 3.2.

There are several empirical correlations for capillary pressure. One of the most commonly used is Skjæveland correlation.

Skjæveland et al. (2000) formulated an expression for mixed-wet system based on Brooks and Corey (1966) correlation. Brooks and Corey correlation is suitable for strongly water-wet rock. The correlation is given as:

$$P_c = \frac{c_w}{\left(\frac{S_w - S_{wir}}{1 - S_{wir}} \right)^{a_w}} \tag{6}$$

where c_w, a_w are curvature parameters, S_w is water saturation, S_{wir} is irreducible water saturation.

Skjæveland et al. (2000) argues that Brooks and Corey can be used for strongly oil-wet rock with some adjustment as shown below:

$$P_c = \frac{c_o}{\left(\frac{S_o - S_{or}}{1 - S_{or}}\right)^{a_o}} \tag{7}$$

where c_o, a_o are curvature parameters, S_o is oil saturation, S_{or} is irreducible oil saturation.

Hence, rock with wettability state in-between these two extreme can use the following correlation:

$$P_c = \frac{c_w}{\left(\frac{S_w - S_{wir}}{1 - S_{wir}}\right)^{a_w}} + \frac{c_o}{\left(\frac{S_o - S_{or}}{1 - S_{or}}\right)^{a_o}} \tag{8}$$

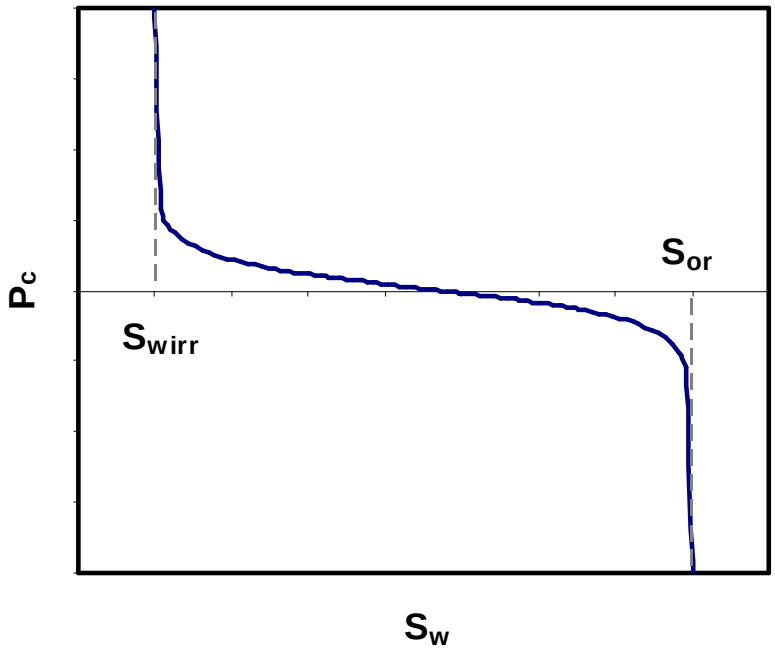

Figure 3.2 Illustration of analytical capillary pressure curve

Equation 8 can be used for both primary drainage and imbibition process using different set of coefficient. Primary drainage process is modeled using $c_o = 0$ and c_w equals to capillary entry pressure.

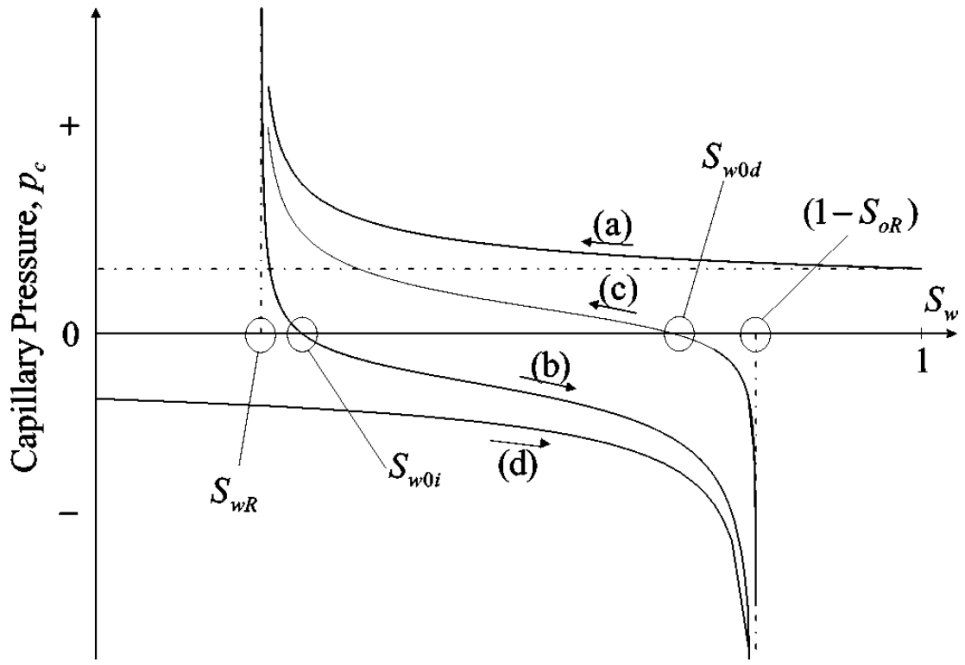

Figure 3.3: Schematic of capillary pressure curves as function of water saturation (a) primary drainage; (b) imbibition; (c) secondary drainage; (d) primary imbibition. Courtesty of Skjæveland et al. (2000).

3.2 Relative permeability

In a multiphase flow, different phases will tend to hinder each other. Some fluids might experience a reduced permeability compared to the flow potential that it would have given it is the only phase in the porous medium. This permeability is called effective permeability while the ratio of effective permeability to the absolute permeability is called relative permeability.

$$k_{ri} = \frac{k_{eff,i}}{k} \tag{9}$$

Darcy's law can still be applied in multiphase flow with some modifications. Effective permeability of a specific phase should be used instead of absolute permeability, resulting in a slightly transformed Darcy's equation:

$$q_i = \frac{k_{eff,i} \cdot A}{\mu_i} \frac{dp}{L} = \frac{k \cdot k_{ri} \cdot A}{\mu_i} \frac{dp}{L} \quad (10)$$

The relative permeability is often displayed graphically as a function of the saturation of the wetting phase, as shown in figure 3.4.

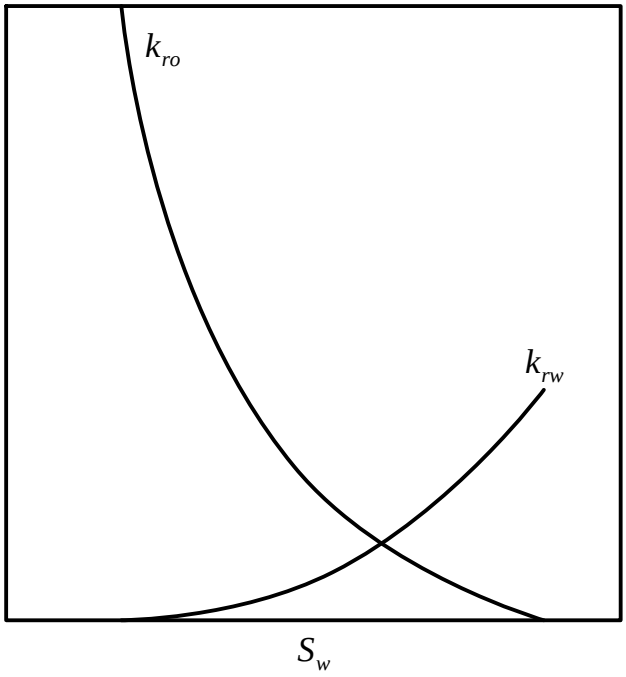

Figure 3.4: Illustration of analytical relative permeability curve

In the absence of laboratory data, empirical correlation can be used as an important tool. For any particular model, we can use different sets of relative permeability curves and investigate the effect of different relative permeability curves on recovery profile.

Another usage of empirical correlation is history matching of production data. We can perform simulation of core flooding experiment using different sets of empirical model parameter and pick up the best match for a given case.

3.2.1 Corey relative permeability

The most well known relative permeability correlations is the Corey (1954) model which is power law of normalized water saturation S_{wn}

$$S_{wn}(S_w) = \frac{S_w - S_{wir}}{1 - S_{wir} - S_{orw}} \tag{11}$$

Corey correlations of relative permeability for oil and water (oil-water system) are

$$k_{rw}(S_w) = (k_{rw})_{S_{orw}} \cdot (S_{wn}(S_w))^{n_w} \tag{12}$$

$$k_{row}(S_w) = (k_{row})_{S_{wir}} \cdot (1 - S_{wn}(S_w))^{n_{ow}} \tag{13}$$

where n_w and n_{ow} are empirical parameters which can be obtained from measurement data, $(k_{rw})_{S_{wi}}$ is end point of water relative permeability, $(k_{row})_{S_{orw}}$ is end point of oil relative permeability for oil-water system.

Corey correlation for gas-oil system are given as

$$k_{rg}(S_g) = (k_{rg})_{S_{org}} \cdot \left(\frac{S_g - S_{gr}}{1 - S_{gr} - S_{wirr} - S_{org}} \right)^{n_g} \tag{14}$$

$$k_{rog}(S_g) = (k_{rog})_{S_{o\max}} \cdot \left(\frac{1 - S_g - S_{org} - S_{wirr}}{1 - S_{org} - S_{wirr}} \right)^{n_{og}} \tag{15}$$

where n_g and n_{og} are empirical parameters, similar with n_w and n_{ow}, $(k_{rg})_{S_{org}}$ is the end-point gas relative permeability, $(k_{rog})_{S_{o\max}}$ is the end-point oil relative permeability for oil-gas system.

3.2.2 LET relative permeability

The Corey correlation has limited degree of freedom. The LET-correlation (Lomeland et. al (2005)) adds more degrees of freedom in order to accommodate the shape of measured relative permeability curves in SCAL experiments.

The LET-type approximation is described by three parameters L, E and T. The correlations for oil and water relative permeability for oil-water system are

$$k_{rw}(S_w) = \frac{(k_{rw})_{S_{wi}} \cdot S_{wn}^{\ L_w}}{S_{wn}^{\ L_w} + E_w \cdot (1 - S_{wn}(S_w))^{T_w}} \tag{16}$$

$$k_{row} = \frac{(1 - S_{wn}(S_w))^{L_o}}{(1 - S_{wn}(S_w))^{L_o} + E_o \cdot (S_{wn}(S_w))^{T_o}} \tag{17}$$

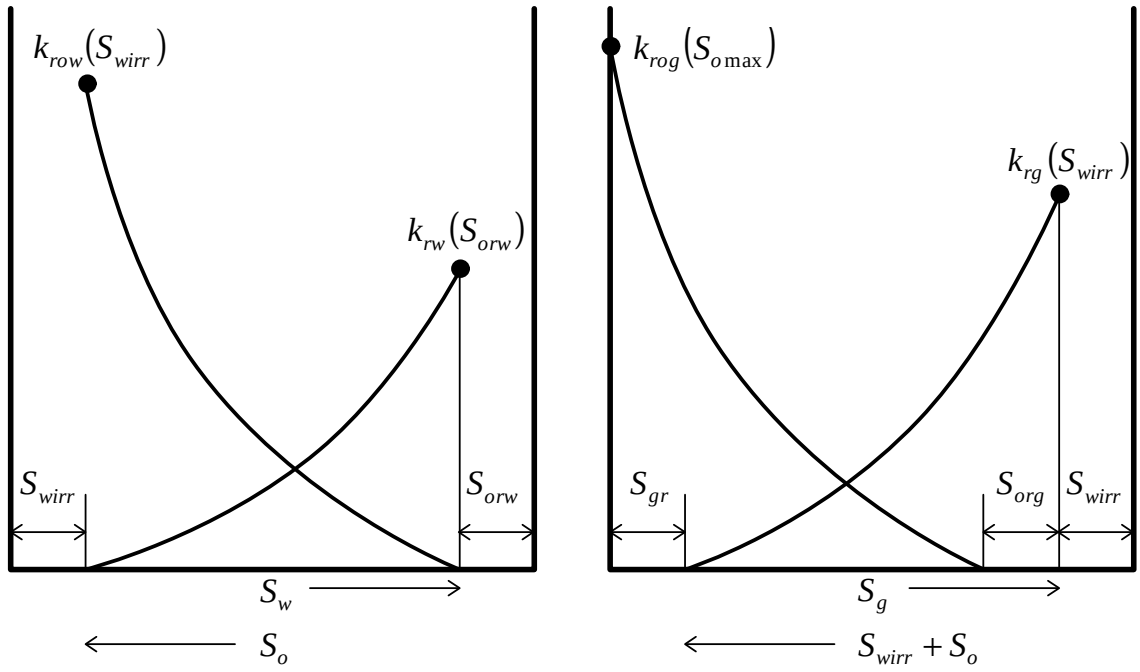

Figure 3.5: Corey relative permeability for oil-water system (left) and oil-gas system (right)

LET correlation for oil-gas system are

$$k_{rg}(S_g) = (k_{rg})_{S_{org}} \frac{\left(\frac{S_g - S_{gr}}{1 - S_{gr} - S_{wirr}}\right)^{L_g}}{\left(\frac{S_g - S_{gr}}{1 - S_{gr} - S_{wirr}}\right)^{L_g} + E_g\left(\frac{1 - S_g - S_{org} - S_{wirr}}{1 - S_{org} - S_{wirr}}\right)^{T_g}} \tag{18}$$

$$k_{rog}(S_g) = (k_{rog})_{S_{gc}} \frac{\left(\frac{1 - S_g - S_{org} - S_{wirr}}{1 - S_{org} - S_{wirr}}\right)^{L_o}}{\left(\frac{1 - S_g - S_{org} - S_{wirr}}{1 - S_{org} - S_{wirr}}\right)^{L_o} + E_o\left(\frac{S_g - S_{gr}}{1 - S_{gr} - S_{wirr}}\right)^{T_o}} \tag{19}$$

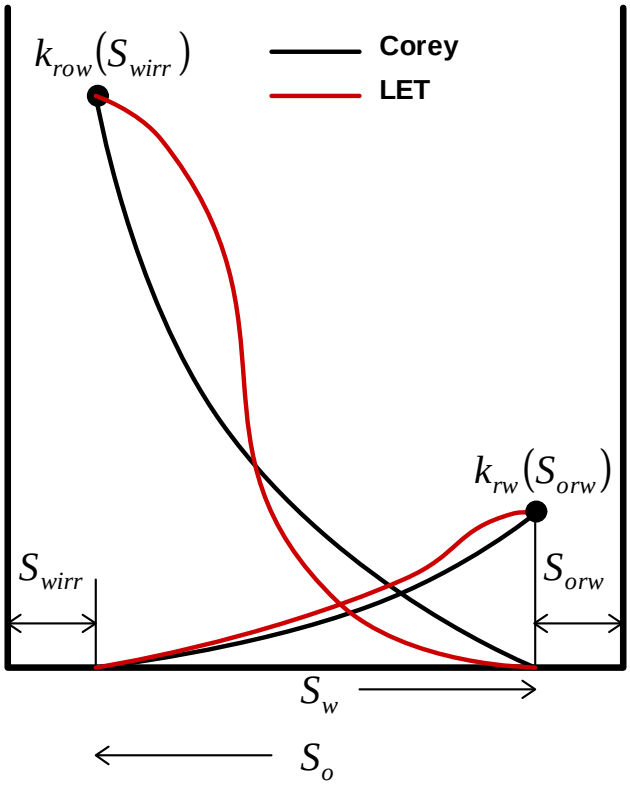

Figure 3.6: Illustration of Corey and LET relative permeability

3.3 Hysteresis

Hysteresis refers to irreversibility or path dependence of the relative permeabilities and capillary pressures on saturation path and saturation history. In two-phase flow, this path dependence process is divided into two process, drainage and imbibition. Drainage is defined as the process in which wetting phase is being displaced by non-wetting phase while imbibition is defined as the process in which wetting phase is displacing non-wetting phase.

Hysteresis has at least two sources, contact angle hysteresis and trapping of the non-wetting phase.

3.3.1 Contact angle hysteresis

Laboratory experiments have demonstrated that the contact angle of a system experiencing drainage is smaller than the contact angle of the same system when experiencing imbibition (Zolotukhin and Ursin (2000)). This phenomenon is typically referred to as the contact angle hysteresis which indicates that parameters of system is depending upon process direction.

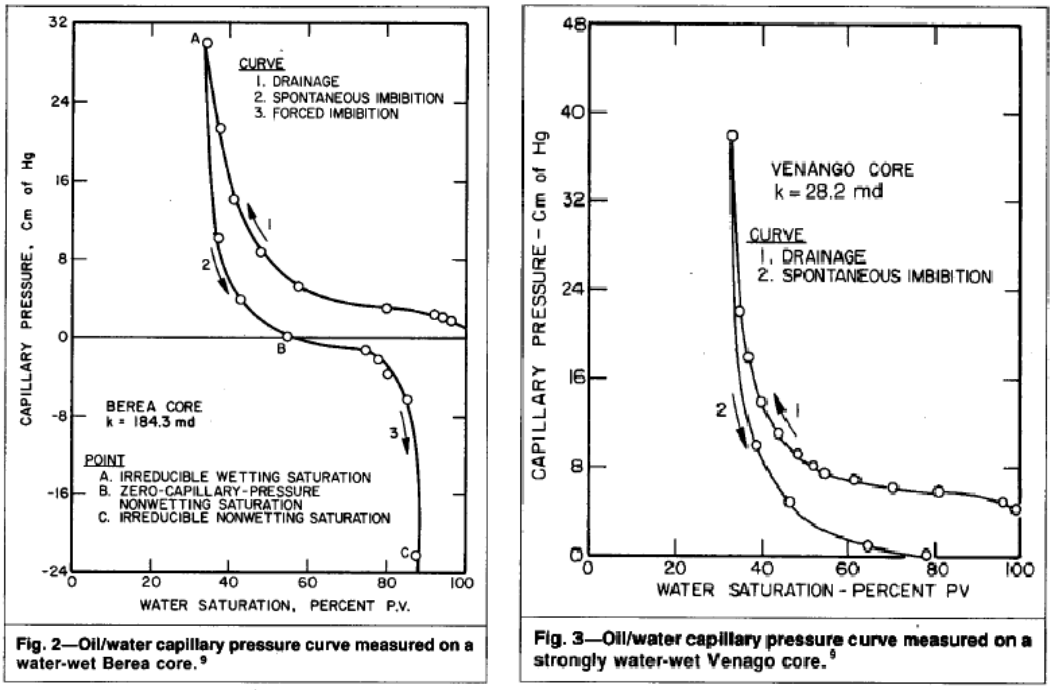

Figure 3.7: Example of contact angle hysteresis for a strongly water-wet and a water-wet core. Adapted from Anderson (1987a).

The derivation of Young's equation assumes that the solid surface is smooth, homogeneous, rigid, and chemically and physically inert with respect to the liquids employed (Lam et al. (2002)). In the ideal situation a unique contact angle would be expected for a given system. However, in a real system a range of contact angles exists. The upper limit of the range is referred to as the advancing contact angle, found at the advancing edge of a liquid drop, while the receding contact angle is found at the receding edge. The contact angle hysteresis is thus the difference between these contact angles (Lam et al. 2002).

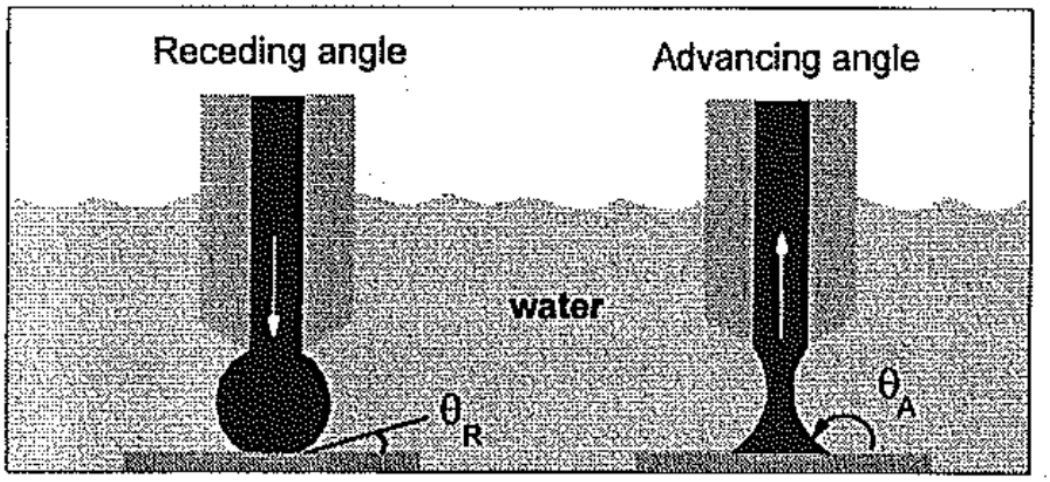

Figure 3.8: Contact angle hysteresis. Adapted from Buckley (1996).

3.3.2 Trapping

Hysteresis can also be caused by trapping. During a flooding process, phases can be trapped in the porous medium causing the process to be irreversible. There are two models explaining the trapping mechanism: the pore doublet model and the snap-off model.

The pore-doublet model explains how fluids can be trapped when the fluids flow at different velocity through pores of different sizes. The capillary forces will pull the wetting fluid into the small pores, but the viscous forces will give a higher velocity through the larger pores. The competition between these two forces will lead to trapping in either the small or large pores. Figure 3.9 illustrates a process with low injection rate dominated by capillary forces. The wetting phase flows at a larger velocity through the smaller pores, and the non-wetting phase is trapped in the larger pores.

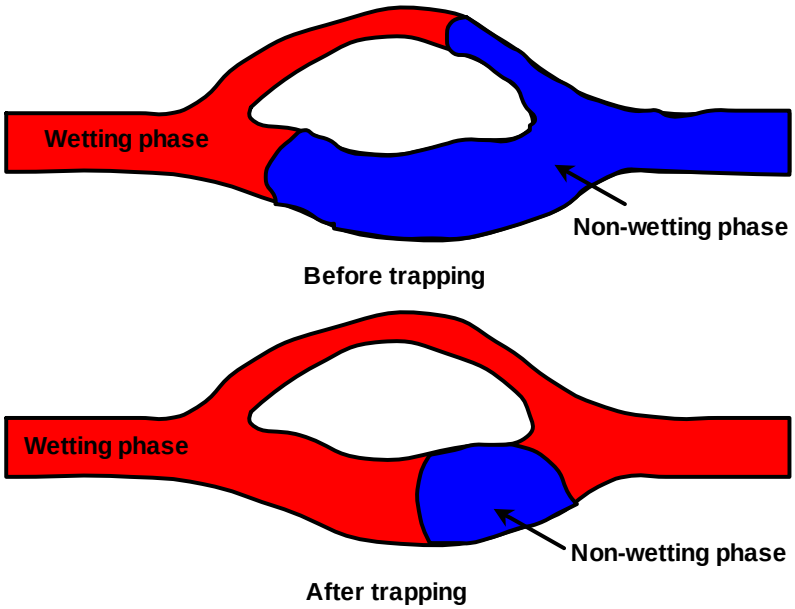

Figure 3.9: Illustration of pore doublet trapping model

The snap-off model explains how fluid can be trapped if the aspect ratio, the relation between the size of the pore body and the pore throat, is high. In water-wet pores the oil can be trapped if the collar of water in the pore throat expands and meets in the middle, as seen in figure 3.10. The oil in the pore is then no longer connected to the rest of the oil-phase and cannot escape from the pore.

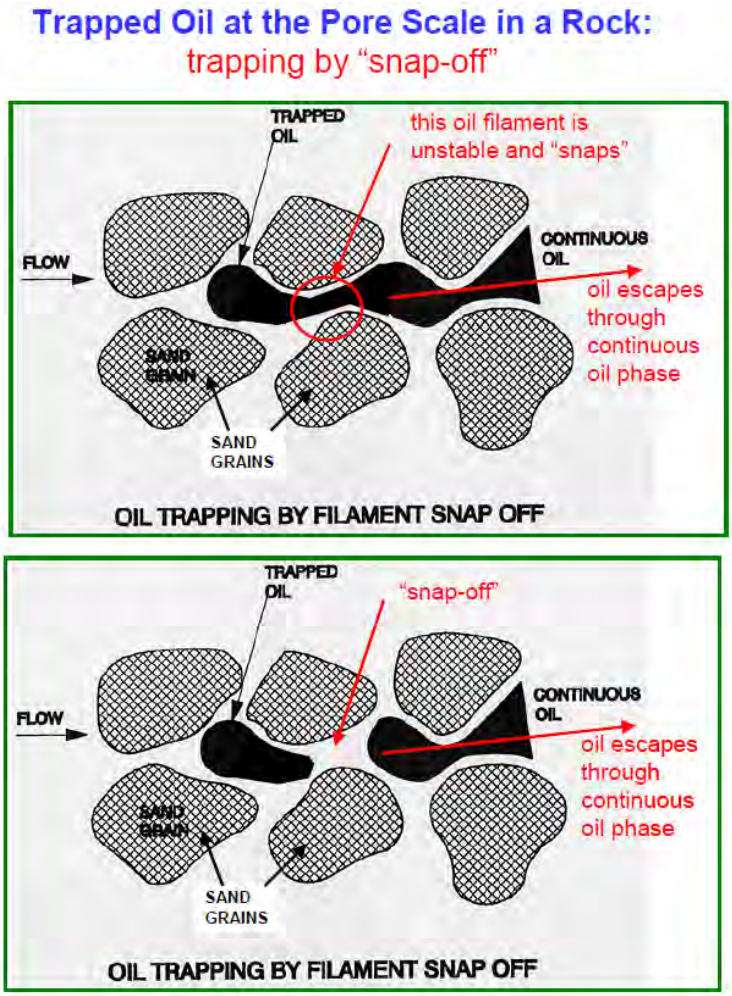

Figure 3.10: Illustration of Snap-off trapping model. Adapted from Sorbie, K. S., van Dijke, M.I.J. (2004).

4. Network Model

Network model offers an alternative approach towards the calculation of single and multiphase flow properties by explicitly incorporating interconnected pore elements into a three-dimensional frame work. Experiment data can be used to anchor a network model and the anchored model can be used further for prediction, for example interpolation and extrapolating sparse and expensive measured data from laboratory.

We use network model in this study to generate two-phase (water-gas) relative permeability and two-phase (water-gas) capillary pressure for CO_2 sequestration study. In addition, we also generated three-phase capillary pressure surface for three-phase flow study for different wettability condition.

A 3D network model for describing three-phase behavior was constructed at Heriot-Watt. The network model is based on “3R approach” which is basically defining pore properties such as capillary entry pressure, pore volume, pore conductance, based on its effective pore radius.

$$P_c \propto \frac{1}{r} \tag{20}$$

$$V \propto r^{v} \tag{21}$$

$$g \propto r^{\lambda} \tag{22}$$

where V is the pore volume, v is the volume exponent, g is the pore conductance and λ is the conductance exponent.

4.1 Pore size and pore geometry

Network model is in three dimension with several bounds (maximum 6 bounds for three-dimension network model) at each direction. The size of the pores radius is assigned randomly from a realistic pore size distribution (PSD). The most common pore size distribution is power law distribution.

$$f(r) \propto r^{k} \tag{23}$$

where k is power law exponent.

Equation 24 implies that there is a larger density of smaller pore size if power law exponent is above zero. If power law exponent is below zero, a large amount of the pore size will be close to maximum pore size.

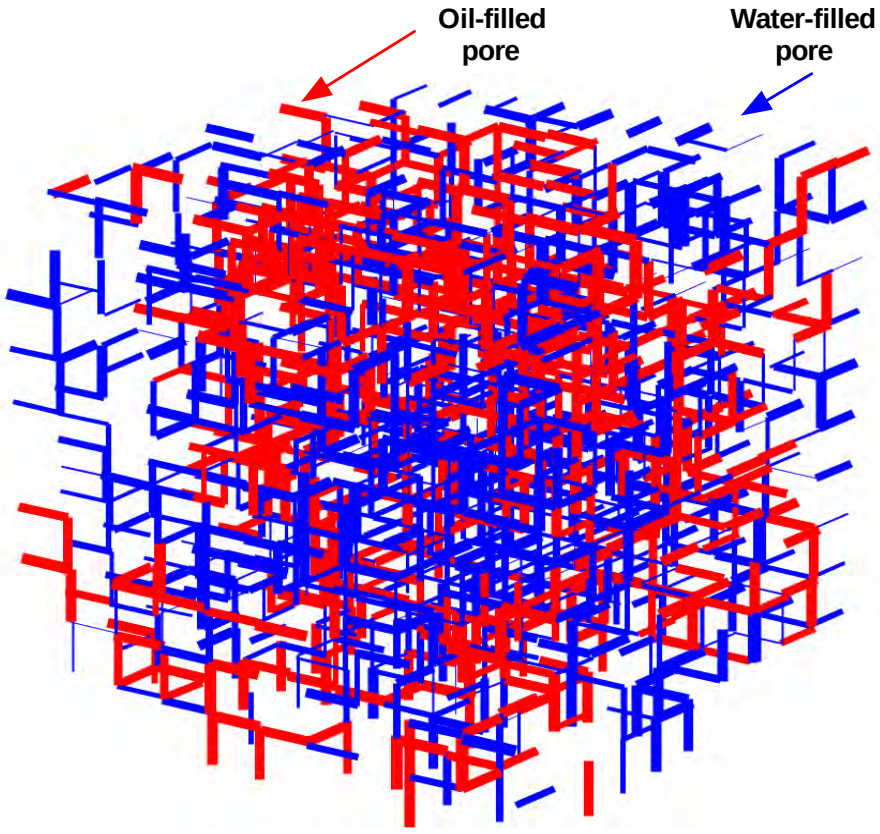

Figure 4.1: Three dimension network model

The connectivity between pores is determined as coordination number. The value for coordination number is typically ranged from 2.5 to 6 for 3D network. The highest coordination number refers to a situation where each pore is connected to the other pores.

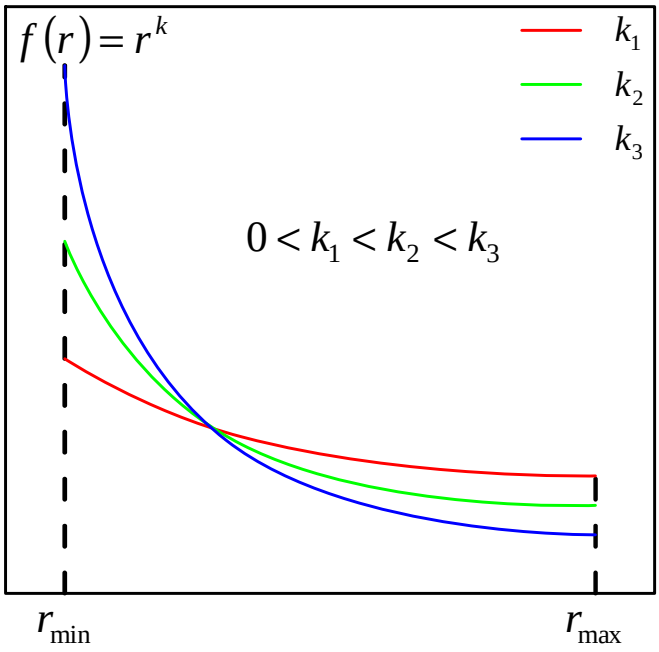

Figure 4.2: Exponential pore size distribution

4.2 Wettability Distribution

The network model can use either fractional-wet or mixed-wet distribution. Contact angle between oil and water phase is defined directly in the model as function of pore radius. In addition, the model allows a different contact angle distribution after primary drainage to imitate ageing process.

Contact angle for both oil-gas and gas-water are calculated using Bartel and Osterhof (1927) equation. The general formulation is

$$\cos\theta_{go} = \frac{1}{2\sigma_{go}}\left\{C_{S,o}\cos\theta_{ow} + C_{S,o} + 2\sigma_{go}\right\} \tag{24}$$

$$\cos\theta_{gw} = \frac{1}{2\sigma_{gw}}\left\{\left(C_{S,o} + 2\sigma_{ow}\right)\cos\theta_{ow} + C_{S,o} + 2\sigma_{go}\right\} \tag{25}$$

where

$$C_{S,o} = \begin{cases} \sigma_{gw} - \sigma_{go} - \sigma_{ow} & \text{if } \sigma_{gw} - \sigma_{go} - \sigma_{ow} < 0 \\ 0 & \text{if } \sigma_{gw} - \sigma_{go} - \sigma_{ow} > 0 \end{cases} \tag{26}$$

4.3 Displacement sequences

Initially, network model is initialized with 100% pores filled with a certain fluid which is usually water. In this case, pores are normally defined as strongly water-wet as observed in real experiment data.

Displacement will be started by increasing displacing phase pressure to a certain level so that pressure difference between the displacing phase and the displaced phase exceeds the minimum capillary entry pressure of the system. In the case of primary drainage process, oil will start to displace water in the pores when pressure difference between oil phase and water phase has exceeded minimum oil-water capillary entry pressure, corresponding to the largest pore throat in the network.

This statement can be explained by considering the Young-Laplace equation of the capillary pressure:

$$P_{cow} = P_{oil} - P_{water} = \frac{2\sigma_{ow}\cdot\cos\theta_{ow}}{r} \tag{27}$$

where σ_{ow} is the oil-water interfacial tension (IFT), θ_{ow} is the contact angle between oil-water mineral surface and r is the pore radius.

Considering this equation, it is obvious that whether or not oil occupies a given pore depends directly on the IFT, contact angle, and the effective pore-throat radius. According to Sorbie and Dijke (2004), although a pore could be occupied by the non-wetting phase at a given pressure, there are two reasons why it is prevented from invading that given pore:

1. That particular pore may be inaccessible which means that there are no neighboring pores already filled with the non-wetting phase. Hence a water-wet pore may not be invaded by oil unless the pressure difference between oil and water is above the capillary entry pressure of the given pore, and the oil phase can access the pore.

2. The wetting phase being displaced is trapped (hydraulically disconnected from the outlet)

Assuming full accessibility, capillary breakthrough will occur when the overpressure in the reservoir, the difference between the pressure of the injected CO_2 phase and the water phase, exceeds the smallest capillary entry pressure in the system

4.4 Anchoring netwok model to experiment data

In this thesis, we need to generate three-phase capillary pressure surface that can be used in reservoir simulation. It is important that network model is the correct representation of the rock in the formation hence some efforts were done on anchoring network model to experiment data.

Manual anchoring requires a lot of trial and error as there is numerous of parameters involved and some of the parameters affect the other parameters. Hence we need a robust and automatic anchoring procedure.

Experimental design and ensemble Kalman-filter were tested for this purpose. Although these techniques were designed to solve linear problem, we have seen that it

also works for non-linear problem as in this case. In order to simplify the problem, we matched experiment data in two steps, primary drainage process and imbibition process.

During primary drainage, wettability model is rather simple. Usually, it only has one type of wettability, strongly water-wet system. Hence we can tune pore geometry parameters in addition to wettability model to match primary drainage data.

Using matched geometry parameters, we can tune on rock wettability after ageing to match capillary pressure during imbibition process.

4.4.1 Experimental Design

Experimental design is a technique which allows us to identify which parameters are the most influential and quantify their impact in a systematical matter. In our case, we can use experimental design to evaluate which parameters that need to be tuned in order to get a good match experiment capillary pressure data and capillary pressure generated from network model.

Since there are too many parameters involved, performing the experiments for all the possible parameters is not feasible as it is time consuming. Moreover, it is difficult to isolate the effect of each parameter as well as the possible interaction between those parameters. Using experimental design, coupled with response surface methodology (RSM), we can analyze the impact of each parameter on capillary pressure matching process in an efficient and rigorous way.

The main idea of RSM is to use a sequence of experimental design to obtain an optimal response (objective function). The model is easy to estimate and apply even with little knowledge about the process involved. Due to its generality, it can only be used as an approximation model.

The first step of experimental design is to identify the uncertainty of each parameters and objective function. The following objective function is used to perform capillary pressure matching.

$$y = \sum \frac{\left| p_{cow\,experiment} - p_{cow\,network\_model} \right|}{p_{cow\,experiment}} \tag{28}$$

Due to number of parameters involved, we did not investigate interaction between parameters. Hence quadratic model was chosen for our RSM model.

$$y = a_1 x_1 + a_2 x_2 + ... + a_n x_n + a_{11} x_1^2 + a_{22} x_2^2 + ... + a_{nn} x_n^2 \tag{29}$$

where $a_1, a_2, ..., a_{11}, a_{22}, ..., a_{nn}$ are constant coefficients obtained by fitting a set of objective function.

Sufficient number of network model simulations must be performed to fit this model. In addition, parameters used in these simulations must be representative to domain of parameter uncertainties. For such problem, we can use optimal design technique, a class of experimental design, which is optimal with respect to some statistical criterion.

Optimal design reduce the costs of simulation by allow statistical model to be estimated with fewer simulation runs. It is known that the least square estimator minimizes the variance of mean-unbiased estimators which corresponds to maximizing the information matrix. For this study, we generate estimator matrix using MATLAB library based on D-optimality criterion. This method tries to minimize $\left| (X'X)^{-1} \right|$ which is equivalent to maximize the determinant of information matrix $X'X$ of the design. The output of optimal design will be the parameter input for network model simulation.

Once the RSM model has been fitted, we use the coefficients $(a_1, a_2, a_3, ..., a_n)$ from RSM model to determine the shifting in parameter domains. Parameters with highest

absolute coefficient are adjusted using bisection technique. The adjustments are defined using the following equation:

$$x_{i\ \min} = \begin{cases} x^0_{i\ \min} & a_i > 0 \\ \dfrac{x^0_{i\ \min} + x^0_{i\ \max}}{2} & a_i < 0 \end{cases} \tag{30}$$

$$x_{i\ \max} = \begin{cases} x^0_{i\ \max} & a_i < 0 \\ \dfrac{x^0_{i\ \min} + x^0_{i\ \max}}{2} & a_i > 0 \end{cases} \tag{31}$$

where $x^0_{i\ \min}, x^0_{i\ \max}$ are minimum and maximum value of parameter i from previous time step. Network model simulation is run with updated parameter range to check for capillary pressure match. The process can be repeated until we get a good match or all the parameters are converged.

4.4.2 Ensemble Kalman-filter

The ensemble Kalman filter (EnKF) is a recursive filter which is suitable for problems with a large number of variables, such as discretization of partial differential equation in geophysical models. This technique is based on Monte Carlo method where the probability distribution is represented by an ensemble of model realizations. EnKF tries to minimize the mismatch between capillary pressure computed by network model with measured capillary pressure.

In general, ensemble Kalman-Filter consists of two steps, forecasting and assimilation. During forecasting step, we run network model for each ensemble to a certain saturation level and extract capillary pressure at that particular saturation level. Afterward, we apply the Kalman equations on output of these runs and measurement data and update the model variables. This step is called assimilation step.

In every saturation level one more measurement is match and the variation in the distribution of the parameters will hopefully decrease as the prior is combined with the likelihood calculated from this new information. Output from the method is distribution of the input parameters to network model.

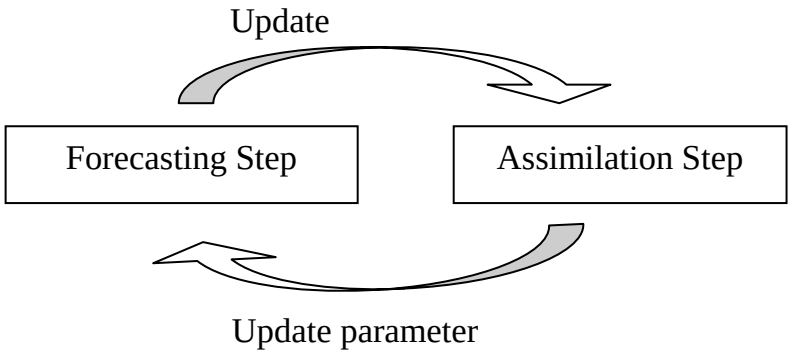

Figure 4.3: Illustration of the Kalman-Filter cycle

As describe above, we start the technique by obtaining measurement for every saturation level. In this case, we have $p_{cow}^{(t)}$ for the oil-water capillary pressures, where t denotes the time step where the data point at saturation $s_w^{(t)}$ is matched. In addition, we have $s_{wir}^{(t)}$ which is constant any time step.

In this study, we assume measurement errors to be within ± 10% with 90% confidence and the error follows a normal distribution, which means that there is a standard deviation $\sigma^{(t)}$ of approximately 6% of the measured value for each type, assuming tails on both sides. Assuming that errors in capillary pressure measurement are independent with error from irreducible water saturation measurement, we will have a diagonal covariance matrix E with elements:

$$e_{k,j} = \begin{cases} \sigma_k^2 & \text{if } k = l \\ 0 & \text{otherwise} \end{cases} \quad \text{for} \quad k,l \in [1,2] \tag{32}$$

According to Evensen (2007), we need to add perturbation on measurement data across the ensemble in order to get a correct sampling. We achieve it by adding stochastic noise from the measurement distribution.

$$\begin{matrix} d_{1,j}^{(t)} = p_{cow}^{(t)} + \xi_{1,j}^{(t)} \\ d_{2,j}^{(t)} = s_{wi}^{(t)} + \xi_{2,j}^{(t)} \end{matrix}, \qquad \text{for} \quad j \in [1,n] \tag{33}$$

where $\xi_{j1}^{(t)}, \xi_{j2}^{(t)}$ are normal distributed with new variance of $\sigma^{(t)}$ for each time step t, with n being the ensemble size:

Since we do not have any information about distribution of our input parameters, we have chosen that the parameter is uniformly distributed between their lower limits a_i and their upper limits b_i, where each parameter is indexed with $i \in [1,m]$, m is number of parameters that we are going to tune using ensemble Kalman filter. Since enKF is based on assumption that parameters are Gaussian (normal distribution), we need to transform our parameters distribution prior using enKF. We use the inverse normal cumulative distribution function g^{-1} to transform between uniformly distributed values to a set of values θ in a Gaussian space with zero mean and unit standard deviation with elements:

$$\theta_i = g^{-1}\left(\frac{\alpha_i - a_i}{b_i - a_i}\right) \quad \text{for} \quad i \in [1,m] \tag{34}$$

with $\alpha^{(t)}$ be updated estimate at time step t.

Some of the parameter ranges are related to each other. For example, we have one parameter for minimum pore size distribution and the other for maximum pore size distribution. It is necessary to make sure that for each ensemble we have a reasonably correct value i.e. minimum pore size distribution for each ensemble should be lower that maximum pore size for that ensemble. This problem can also occur after an update of the filter. If their intervals are given by $\lfloor a_{\min\_size}, b_{\min\_size} \rfloor$ and $\lfloor a_{\max\_size}, b_{\max\_size} \rfloor$, we can use the following approach to set both minimum and maximum values to the mean of the two:

$$\alpha'_{\min\_size} = \frac{\alpha_{\min\_size} + \alpha_{\max\_size}}{2}$$
$$\alpha'_{\max\_size} = \frac{\alpha_{\min\_size} + \alpha_{\max\_size}}{2} \tag{35}$$

replacing $\alpha_{\{\min\_size,\max\_size\}}$ with $\alpha'_{\{\min\_size,\max\_size\}}$ if $\alpha_{\max\_size} < \alpha_{\min\_size}$. Using this approach, we are adjusting the parameters in the direction that the Kalman filter wants but in a controlled manner such that the maximum value is not smaller than minimum value.

The forward simulation is given by

$$\psi^{(t)} = f\left(\alpha^{(t)}, s_w^{(t)}\right) \tag{36}$$

where f returns capillary pressure ψ when simulation is run with the parameters α towards a target saturation s for time step t.

The EnKF is based on first running the forward model and then updating when new measurements become available. This is done for each ensemble member. Update is done with the standard Kalman filter update equations, combined with an ensemble approximation to the covariance matrices (Evensen (2007)). Introducing the ensemble matrices Θ, Y and D holding the n ensemble members of θ, y and d in each column, the EnKF update equations may be written:

$$\Theta^{(t+1)} = \Theta^{(t)} + K^{(t)}\left(D^{(t)} - Y^{(t)}\right) \tag{37}$$

where $K^{(t)}$ is the Kalman gain matrix given by:

$$K^{(t)} = C_{\Theta Y}{}^{(t)}\left(C_{YY}{}^{(t)} + E^{(t)}\right)^{-1} \tag{38}$$

The covariance used above is given by the standard expressions:

$$C_{\Theta Y} = \frac{1}{n-1}\left(\Theta - \overline{\Theta}\right)\left(Y - \overline{Y}\right)^T$$
$$C_{YY} = \frac{1}{n-1}\left(Y - \overline{Y}\right)\left(Y - \overline{Y}\right)^T \tag{39}$$

where $\overline{Y}$ and $\overline{\Theta}$ are the matrices holding the ensemble means in each column:

$$\overline{\Theta} = \{\overline{\theta}, \overline{\theta}, \overline{\theta}, ..., \overline{\theta}\} = \Theta \cdot 1_n \tag{40}$$

$$\overline{Y} = \{\overline{y}, \overline{y}, \overline{y}, ..., \overline{y}\} = Y \cdot 1_n \tag{41}$$

where 1_n is the n times n matrix with all elements equal to $1/n$.

We start the process by setting up initial ensemble of each parameter stochastically. In this case, we draw values of $\theta_i^{(1)}$ normally distributed with zero mean and unit standard deviation.

If the residual is large, there will be large changes in the parameters. The amount of changes is determined by the Kalman gain. If the distribution of parameters θ and capillary pressure y are width, the covariance matrix $C_{\Theta Y}$ will have large entries. If the entries in the matrices C_{YY} and E are large, this will have the opposite effect. E has large entries if we consider the uncertainties in the measurements to be large. The Kalman gain will therefore depend on the distributions of the parameters and the measurements.

The final solution of network model parameters are taken as the mean of the last ensemble after update. The capillary pressure curve made by the network model with these parameters should match all the measurements according to the given standard deviation.

The approach for Ensemble Kalman-Filter technique that we use in this study is similar to the previous study by Holm et al. (2009). The main difference in the approach is matching of end-point saturation. In this study, we include end-point saturation as measurement parameter. This parameter will be tuned at each time step hence we can get a good fit on end-point saturation. Holm et al. (2009) focused solely on capillary pressure matching and there is no effort made on end-point saturation matching. Instead, they relax the matching criteria for capillary pressure near the asymptote.

Internal report 2 in this thesis discusses application of these two methods to tune network model for capillary pressure matching. In that report, we presented a typical network model and use it as synthetic case with maximum 10% random noise added to the data. The report shows that ensemble Kalman-Filter is superior compared to experimental design for given case.

We have considered several improvements that can be done to enhance both techniques. Details will be presented in Further work section.

5. Three-phase flow characteristic

When the three phases oil, water and gas are present in a porous media at the same time, three-phase flow parameters must be used to describe the behaviour. Three-phase flow properties are very important for correct modelling and prediction of EOR processes that involves water and gas such as WAG and depletion after water flooding.

The description of three-phase flow properties as shown below was included into UTCHEM, a chemical flooding simulator made by University of Texas Austin.

5.1 Three-phase capillary pressure

Killough (1976) method is often used to model three-phase capillary pressure. The three-phase capillary pressure is constructed as a weighted average between the two-phase drainage and imbibition curves.

$$P_c = P_{c\,drainage} + F\left(P_{c\,imbibition} - P_{c\,drainage}\right) \tag{42}$$

$$F = \frac{\left(\frac{1}{S_w - S_{w,hys} + E} - \frac{1}{E}\right)}{\left(\frac{1}{S_{w,\max} - S_{w,hys} + E} - \frac{1}{E}\right)} \tag{43}$$

where $P_{c\,drainage}$ is the drainage capillary pressure, $P_{c\,imbibition}$ is the imbibition capillary pressure, $S_{w,hys}$ is the water saturation at the hysteresis reversal point, $S_{w,\max}$ is the maximum water saturation attainable on the scanning curve when trapping of the other phases is subtracted and E is a curvature parameter.

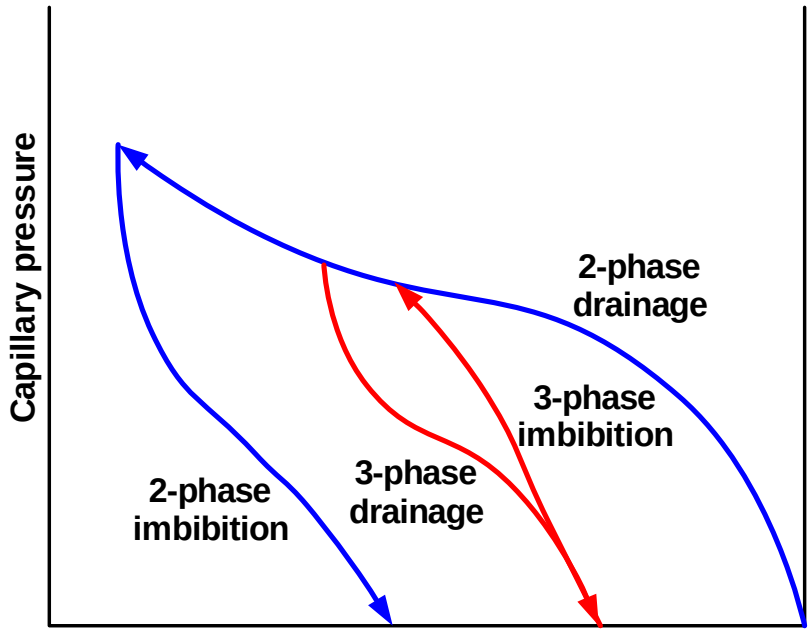

Figure 5.1: Killough three-phase capillary pressure

Helland and Skjæveland (2004) proposed a correlation for three-phase capillary pressure which basically the extension of Skjæveland (2000) capillary pressure correlation. The general formulation of Helland and Skjæveland capillary pressure is as follow:

$$P_{cij} = c_1(1-S_1)^{-d1} + c_2(1-S_2)^{-d2} \tag{44}$$

where P_{cij} is three-phase capillary pressure of oil-water, oil-gas and gas-water, S_1 and S_2 are two dominating phase saturations. The coefficient c and d have to be determined by matching to the three-phase capillary pressure experiment data.

Very few measurements of three-phase capillary pressure exist. Kalaydjian (1992) measured three-phase capillary pressure on an outcrop water-wet core and on unconsolidated material and observed that the three-phase capillary is dependent on all phase saturations. In addition they also found that the three-phase capillary pressure had a higher value than the two-phase capillary pressure, which indicates that Killough correlation could not be used to predict three-phase capillary pressure.

A few attempts have been made to estimate three-phase capillary pressure using network models (Mani and Mohanty (1998), Fenwick and Blunt (1998), Lerdahl et al. (2000), vanDijke and Sorbie (2001)). The network models are usually anchored to the measured two-phase capillary pressure data as discussed in chapter 4.4. The anchored network models are used to predict three-phase capillary pressure. The three-phase capillary pressure surface is obtained by simulating injection of one phase (primary process) until reaching a certain saturation followed by another phase injection (secondary process). The process is repeated for different saturation level. This will give us a collection of saturation paths, which can be used as a based for three-phase capillary pressure surface, as shown in figure 5.2.

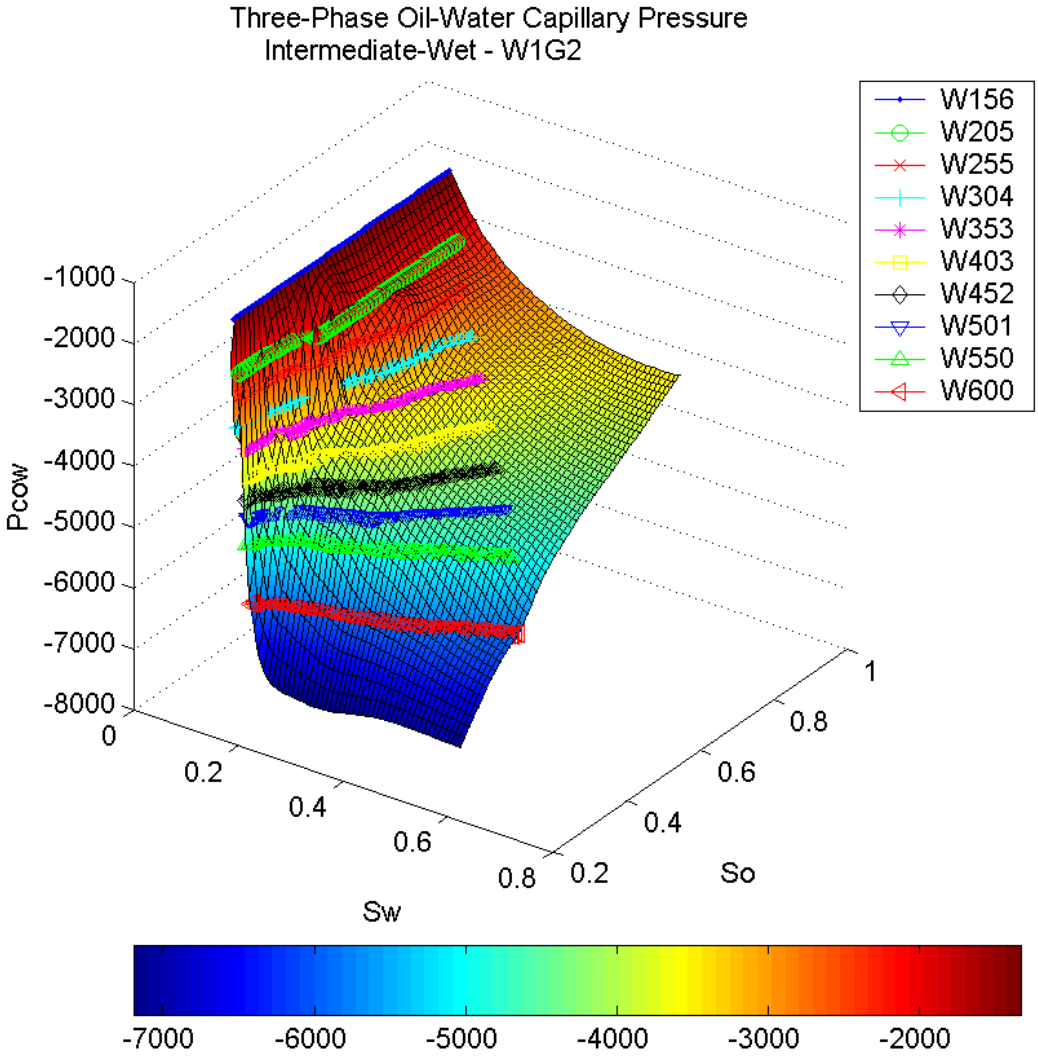

Figure 5.2: Example of three-phase capillary pressure surface for W1G2 process

5.2 Three-phase relative permeability

Three-phase relative permeability is difficult to measure and correlations of two-phase data are usually used to estimate the three-phase data. It is often assumed that the water and gas relative permeability is a function of its own saturation only, and two-phase relative permeabilities for water and gas can therefore be used for three-phase cases. Three-phase oil relative permeability is assumed to be a function of both gas and water saturation.

Many correlations for the oil relative permeability exist. Several authors have made correlations for three-phase relative permeability. The Stone I (Stone (1970)) and Stone II (Stone (1973)) models for estimation of three-phase relative permeability are widely used. Stone introduced the normalised saturations.

$$S_w^* = \frac{S_o - S_{orm}}{1 - S_{wi} - S_{orm}} \tag{45}$$

$$S_w^* = \frac{S_w - S_{wi}}{1 - S_{wi} - S_{orm}} \tag{46}$$

$$S_g^* = \frac{S_g}{1 - S_{wi} - S_{orm}} \tag{47}$$

where S_{orm} is the minimum oil saturation after gas and water injection.

In the Stone I model the relative permeability of oil is defined as

$$k_{ro} = S_o^* \cdot \beta_w \cdot \beta_g \tag{48}$$

β_w and β_g are given by

$$\beta_w = \frac{k_{row}}{1 - S_w^*} \tag{49}$$

$$\beta_g = \frac{k_{rog}}{1 - S_g^*} \tag{50}$$

where k_{row} is the two-phase oil relative permeability in a oil-water system and k_{rog} is the two-phase oil relative permeability in a gas-oil system.

The Stone II (Stone 1973) model defines the oil relative permeability as

$$k_{ro} = (k_{row})_{S_{wi}} \left[\left(\frac{k_{row}}{(k_{row})_{S_{wi}}} + k_{rw} \right) \left(\frac{k_{rog}}{(k_{row})_{S_{wi}}} + k_{rg} \right) - (k_{rw} + k_{rg}) \right] \tag{51}$$

where $(k_{row})_{S_{wi}}$ is the relative permeability of oil at the irreducible water saturation from the two-phase oil-water system.

It is difficult to conduct a three-phase flow experiment. The number of experiments concerning three-phase flow is therefore limited, but some reported cases exist. The experiments show a very complex behavior. Several different results for the hysteresis behavior of gas, water and oil have been reported, where wettability plays an important role. The relative permeability correlations, both Stone I and Stone II, often fail to predict what is seen in the experiments.

In order to describe the experimental data correctly many mechanisms must be included in the model. Larsen and Skauge (1998) have made a history dependent model for three-phase relative permeability (WAGHYST model), which have been included in the Eclipse 100 simulator.

In this model, gas trapping is modeled in the same way as two-phase hysteresis method of Carlson (Carlson (1981)). The imbibition relative permeability is calculated from drainage relative permeability curve in the same hysteresis loop. In this model, gas mobility is reduced in three-phase condition i.e. water saturation is higher than its connate saturation. The relative permeability is reduced by the ratio of connate water saturation divided by actual water saturation.

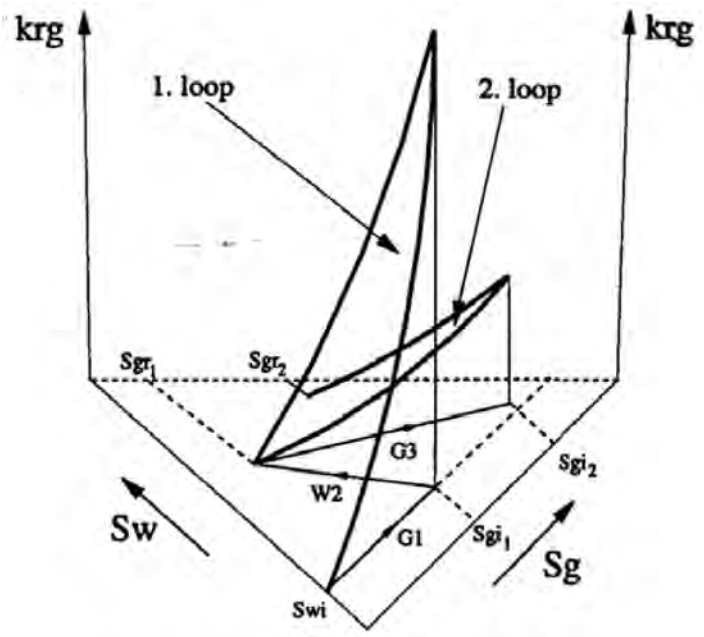

Figure 5.3: Larsen and Skauge three-phase gas relative permeability.

Adapted from Larsen and Skauge (1998).

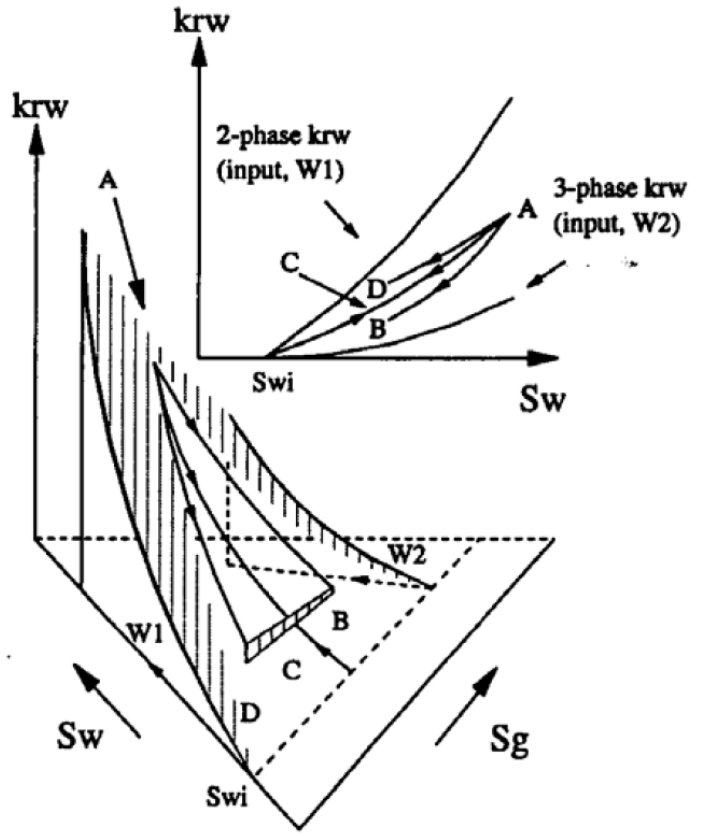

Figure 5.4: Larsen and Skauge three-phase water relative permeability.

Adapted from Larsen and Skauge (1998).

Three-phase oil relative permeability is calculated by Stone 1 method (Stone (1970)) The residual oil saturation is a function of trapped gas saturation which means residual oil saturation could be lower in three-phase dominated zone. This is similar to observation made by Holmgren and Morse (1951), Kortekaas and van Poelgeest (1991) and Skauge and Aarra (1993).

Water relative permeability input in WAGHYST model are divided into two groups, two-phase condition and three-phase condition. For transitions between two-phase and three-phase zones, we calculate water relative permeability using interpolation between these two curves, as illustrated in figure 5.4.

For the purpose of this study, we have implemented Larsen and Skauge three-phase relative permeability model into UTCHEM. This implementation was compared to Eclipse WAGHYST model and gives a very good match. In addition, we have included description of three-phase capillary pressure as 2D table input, similar to Eclipse PCG32D and PCW32D keywords. The input criteria is relaxed compare to Eclipse to allow three-phase capillary pressure input which is higher than two-phase capillary pressure.

The impact of including three-phase capillary pressure is investigated in internal report 1 and paper 1 which can be found in this thesis. In general, we observe a significant effect of three-phase capillary pressure. On the contrary, two-phase capillary pressure give small and relatively negligible effect on recovery profile, according to our simulation result. These results will be elaborated in chapter 8 in this thesis.

6. CO_2 properties

It is important to understand the physical and chemical processes involved when addressing the efficiency of geological storage of CO_2, especially when determining whether or not CO_2 will remain stored under a certain set of condition. This chapter serves as background theory for further discussion on CO_2 sequestration study. The CO_2 properties are modeled internally by CMG-GHG simulator based on equation of state.

6.1 CO_2 physical properties

Figure 6.1 shows CO_2 behavior as function of pressure and temperature. Under normal condition (15 °C, 1 bar) CO_2 is in gas phase. At low temperatures CO_2 is a solid. Increasing temperature, with pressure below 5.1 bars, will cause the solid to sublime directly into the vapor state. At intermediate temperatures (between triple point temperature and critical temperature), CO_2 may turned from vapor into a liquid by compressing it above its liquefaction pressure. At temperatures higher than critical temperature, with pressure above 73.9 bar, CO_2 is in supercritical state. At this condition, pure gaseous CO_2 can not be liquefied regardless of the pressure, and in the supercritical environment only one phase exists. The CO_2 is neither a gas nor a liquid, and is best described as a very mobile liquid. Supercritical CO_2 forms a phase that is distinct from the aqueous phase, and can change continuously into either gaseous or liquid CO_2 with no phase boundaries.

CO_2 density is dependent on its pressure and temperature. As shown in figure 6.2, CO_2 density increased as pressure is increased and decreasing as temperature is raised. At high pressure, CO_2 density can be very high, approach or even exceeding liquid water density (Freund et al. (2005b))

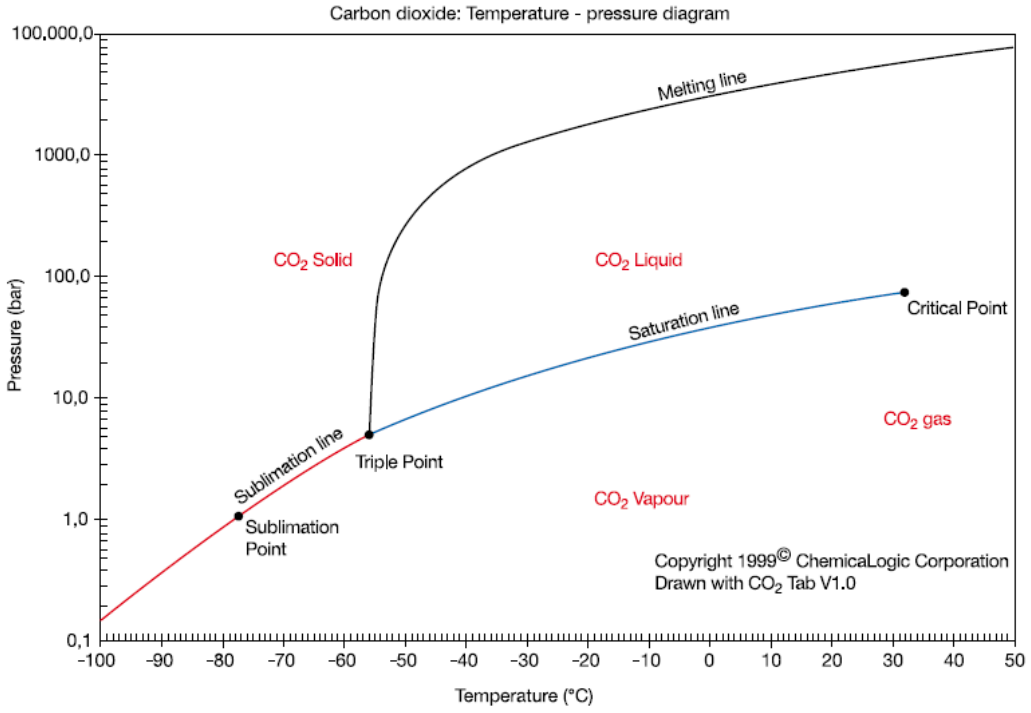

Figure 6.1: Phase diagram for CO_2. Adapted from Rubin et al. (2005).

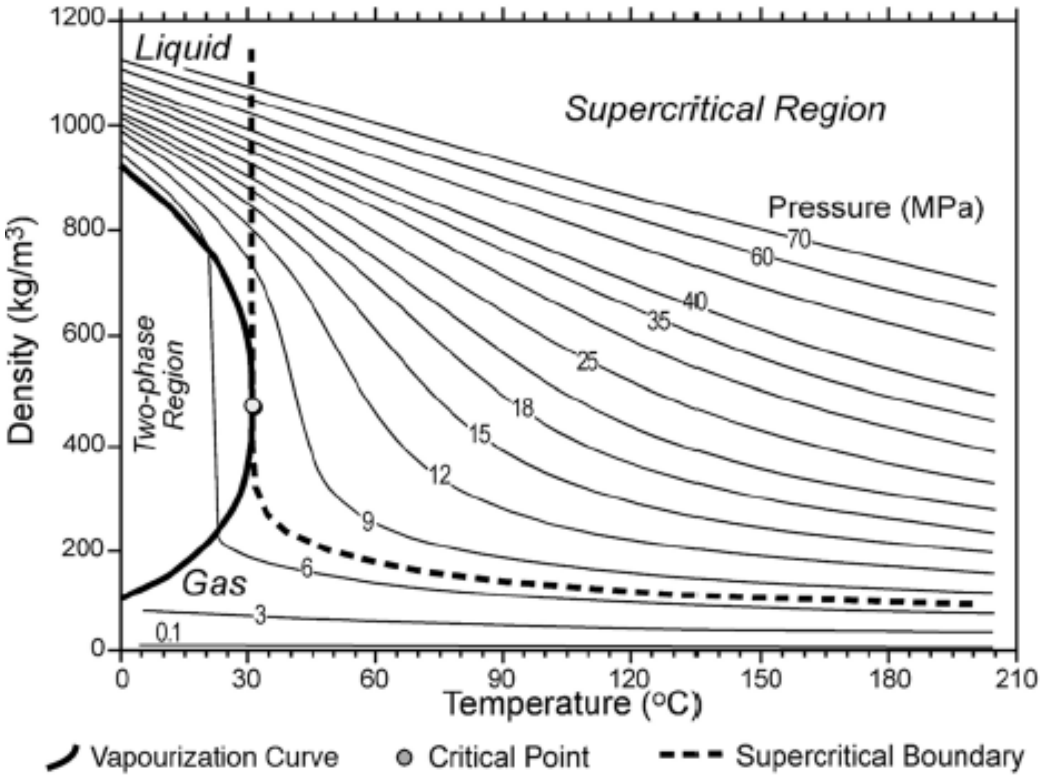

Figure 6.2: Effect of pressure and temperature on CO_2 density.

Adapted from Freund et al. (2005b).

An overview of the physical properties of CO_2 is shown below.

Property	Value
Molecular weight	44.01
Critical temperature	31.1 ^{o}C
Critical pressure	73.9 bar
Critical density	467 kg/m^3
Triple point temperature	-56.5 ^{o}C
Triple point pressure	5.18 bar
Boiling point	-78.5 ^{o}C @ 1.013 bar
Gas Phase	
Gas density @ boiling point	2.814 kg/m^3
Gas density (standard condition)	1.976 kg/m^3
Viscosity @ standard condition	13.72 μPa.s
Solubility in water @ standard condition	1.716 vol/vol
Liquid Phase	
Vapour pressure (20 ^{o}C)	58.5 bar
Liquid density (-20^{o}C, 19.7 bar)	1032 kg/m^3
Viscosity (standard condition)	99 μPa.s
Solid Phase	
Density (freezing point)	1562 kg/m^3

Table 6.1: Physical properties of CO_2

CO_2 saturated brine has higher density compare to pure brine hence it will migrate downward while pure brine will migrate upward. Since CO_2 has lower density than brine, it will also migrate upward. Thus, it will increase the contact between brine and

CO_2, enhance the dissolution rate of CO_2 into brine. Figure 6.3 shows the effect of CO_2 concentration to CO_2 saturated brine density.

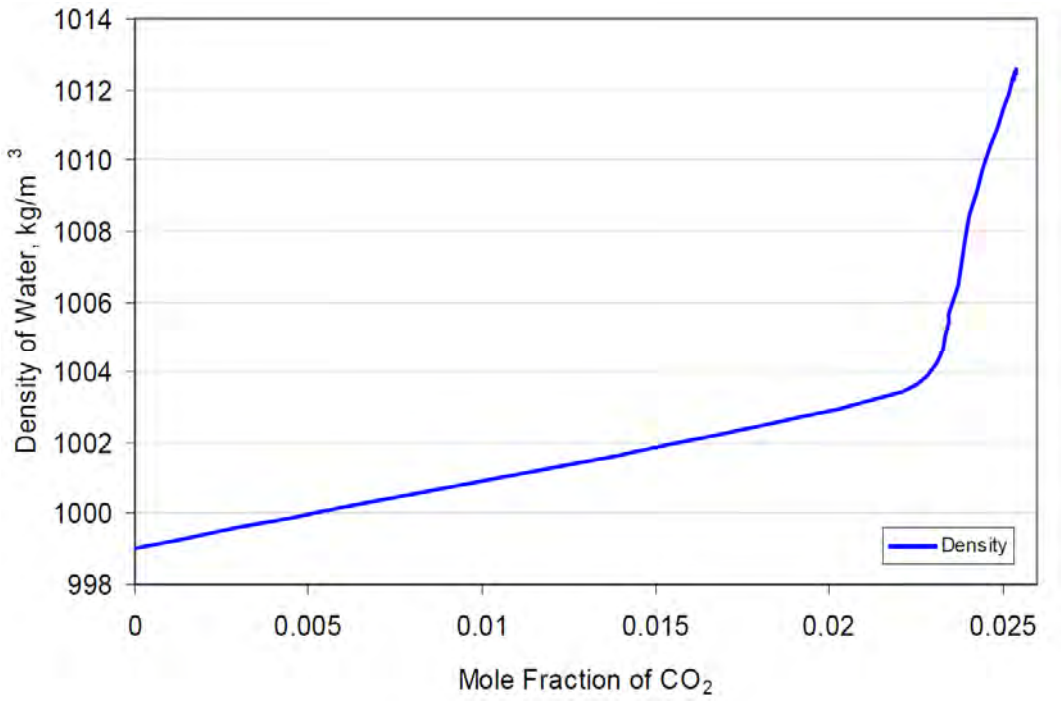

Figure 6.3: Effect of dissolved CO_2 concentration to brine density at 60 ˚C. Adapted from Ülker et al. (2007)

6.2 Solubility

Solubility of CO_2 in water is mainly dependent on pressure and temperature. Figure 6.4 shows the effect of pressure and temperature on CO_2 solubility in water. We can see that solubility of CO_2 increases with increasing pressure and decreases with increasing temperature. Baines and Worden (2004) stated that at temperature above 100 degrees celcius and pressure above 300 bars, CO_2 solubility increases with increasing temperature.

Solubility is also dependent on water salinity. Figure 6.5 shows that an increase in salinity significantly decreases the CO_2 solubility, especially at high pressure.

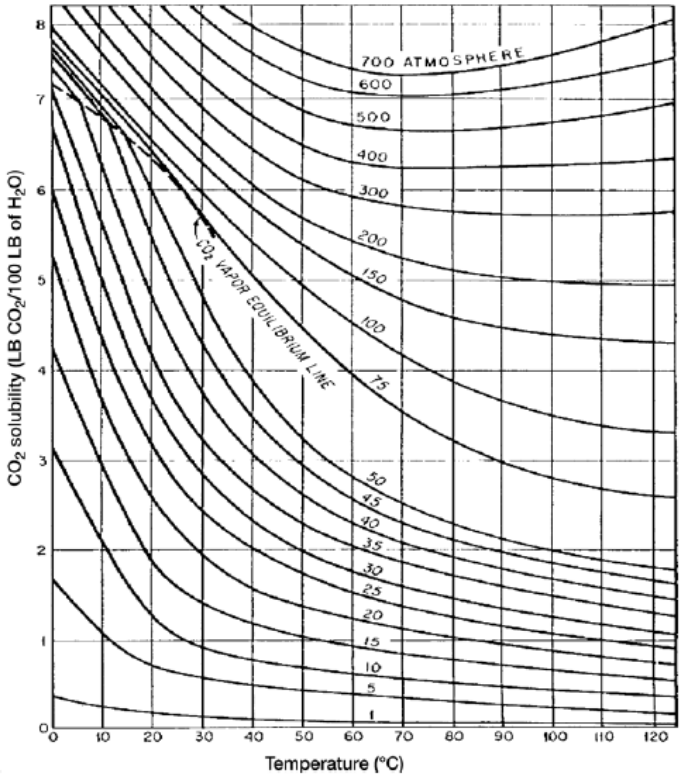

Figure 6.4: Solubility of CO_2 in water (Kohl and Nielsen 1997). Adapted from Freund et al. (2005b).

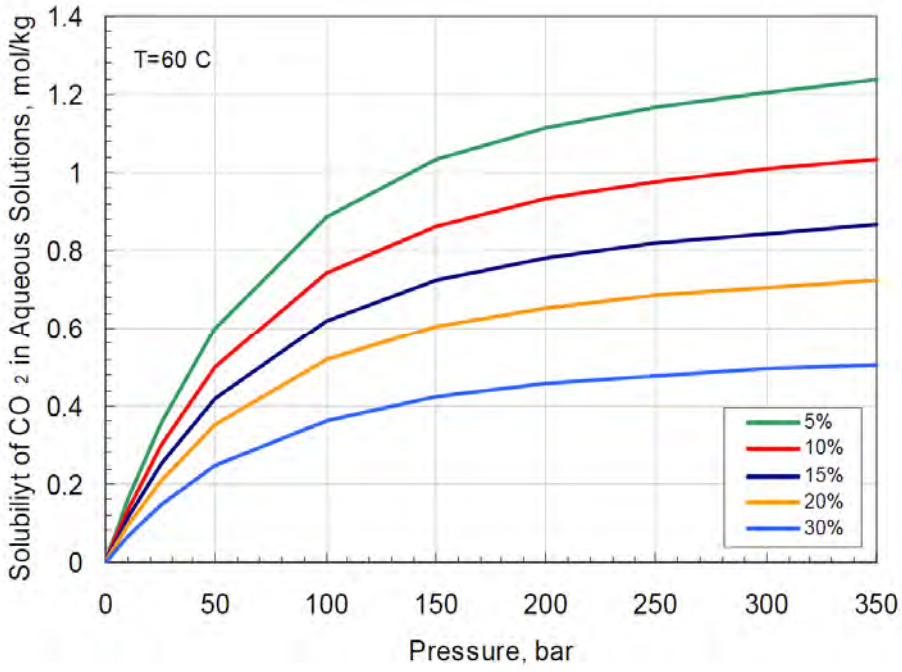

Figure 6.5: Solubility of CO_2 in aqueous solutions of NaCl with varying total salinity at 60 ˚C. Chang et al. 1998. Adapted from Ülker et al. (2007).

6.3 Diffusion

Diffusion describes the spread of particles from regions of higher concentration to regions of lower concentration. The concept of diffusion is tied to that of mass transfer driven by a concentration gradient, but diffusion can still occur when there is no concentration gradient. Diffusion rate is a function of only temperature, and is not affected by concentration.

Tamimi et al. (1994) measured the liquid-phase diffusion coefficient for hydrogen sulphide, carbon dioxide, and nitrous oxide in water over the temperature range 293 – 368K. Tamimi et al. shows that CO_2 diffusion rate is increasing with temperature at increasing slope which means it is more critical issue at higher reservoir temperature.

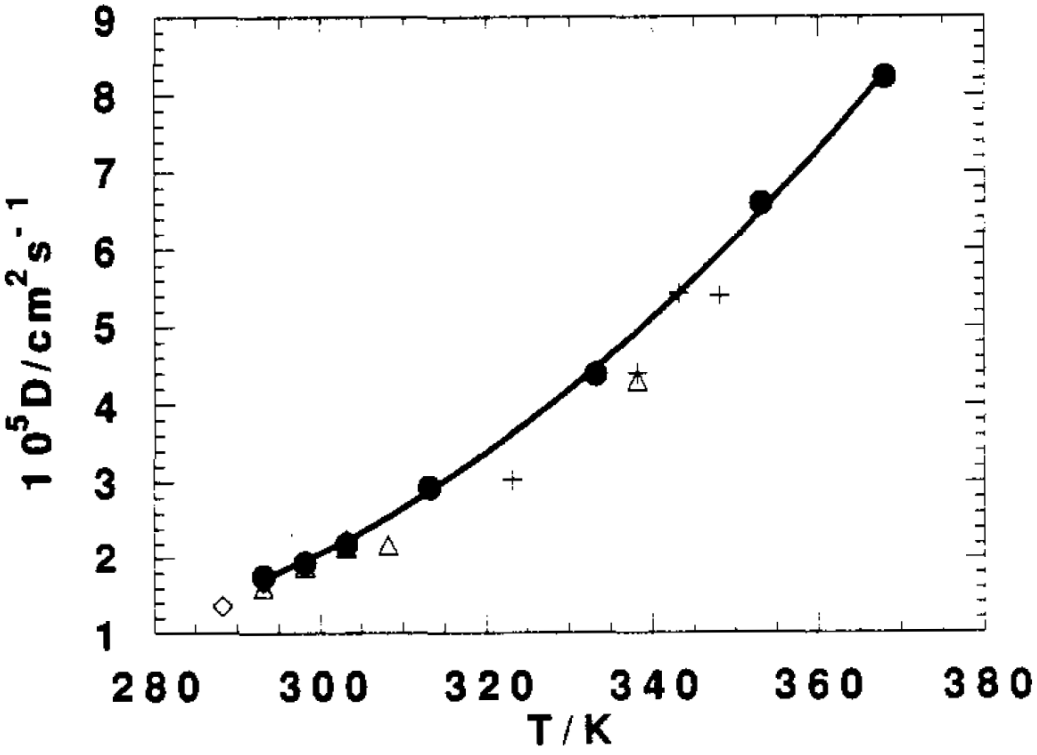

Figure 6.6: Temperature - Diffusivity of CO_2 in water plot.
Adapted from Tamimi et al. (1994)

7. CO_2 sequestration mechanism

During CO_2 sequestration, injected CO_2 will interact with brine and rock minerals both in aquifer and cap rocks. This interaction will affect the properties of all involved compounds and can affect storage capacity of aquifer. It is of great importance to understand mechanisms involved during CO_2 sequestration in order to properly model storage capacity.

In addition, it is shown by several authors that CO_2-brine interfacial tension and rock wettability can be altered during this interaction. One of the focus of this thesis is to properly model alteration in both properties and evaluate the effect to storage capacity.

7.1 CO_2 Flow mechanisms

Johnson et al. (2001) stated that injected CO_2 can be categorized into three distinct processes:

1. Immiscible CO_2 plume migration
2. Interaction between CO_2 plume with ambient saline waters
3. Interaction between CO_2 plume with aquifer and cap-rock minerals

7.1.1 Immiscible CO_2 plume migration

According to Bryant et al. (2006), CO_2 migration is mainly controlled by bouyancy forces, uniformity of the displacement front and saturation of CO_2 behind the front. CO_2 displacing water is essentially an immiscible drainage process. Assuming water-wet state condition, CO_2 will enter largest pores first and increase CO_2 saturation rapidly. This will increase relative permeability of CO_2 and enhance CO_2 injectivity.

As pointed out in chapter 6, CO_2 density is in general lower compared to water density. Hence, the effect of gravity segregation will result in migration of immiscible CO_2 plume upward. In general, saline formation will have an even higher density thus allowing more rapid CO_2 plum migrates upward. Bryant et al. observed in 2006 that the first-order influence on buoyancy-driven CO_2 displacement is heterogeneity of the aquifer, not instability of the CO_2-fluid contact.

Due to low viscosity, hence higher mobility ratio, CO_2 will migrate into high permeability zone. This could result in CO_2 skipping part of the pore space (viscous fingering effect), depending on the heterogeneity and anisotropy of the rock permeability (Benson et al. (2005)). Combination of gravity segregation and viscous fingering could affect CO_2 storage capacity due to low sweep efficiency.

During CO_2 migration through a formation, some of the CO_2 will be trapped in the pore space by capillary forces. This is commonly referred as “residual CO_2 trapping”, which could immobilize significant amounts of CO_2. When CO_2 is injected at the bottom of a thick formation, all of the CO_2 may be trapped by this mechanism, even before it reaches the cap rock (Benson et al. (2005)).

7.1.2 Interaction between CO_2 plume with water

CO_2 is a rather reactive substance. According to Baines and Worden (2004), CO_2 injection into deep subsurface will result in chemical disequilibria and initiate various chemical reactions. Benson et al. (2005) describe possible reactions could include diffusion, dissolution of CO_2 into fluid formation, mineralization and adsorbtion of CO_2 into organic material.

It is very important to address the direction, rate and magnitude of such reactions both in terms of their impact upon the ability of a host formation to contain the injected CO_2 safely, and in terms of the longevity of CO_2 containment. This is certainly not an easy task since these processes depend upon the structure, mineralogy and hydrogeology of the specific lithology concerned (Baines and Worden (2004)).

In general, injected CO_2 is in dry condition. The reason for this is to reduced deterioration of equipment such as tubing and pump. Dry CO_2 also has another benefit as it reduces the risk of CO_2 hydrate forming within the pipes. Injected dry CO_2 gas will interact each other causing both dissolution of CO_2 into water and dissolution of water into CO_2 (Baines and Worden (2004)). The dissolution will follow the following reaction:

$$CO_{2(g)} + H_2O \Leftrightarrow CO_{2(aq)} + H_2O \Leftrightarrow H_2CO_3 \Leftrightarrow HCO_3^- + H^+ \Leftrightarrow CO_3^{2-} + 2H^+ \quad (39)$$

This reaction is dependent on temperature and pressure condition, which are important factors influencing the solubility of CO_2 (Freund et al. (2005a)). This reaction is also dependent upon the ability of the formation to buffer pH. According to le Chatelier's principle, additional reactions that consume H+ ions will tend to drive the above reaction to the right, causing more CO_2 to dissolve (Baines and Worden (2004)).

The CO_2 solubility also depends on the degree of CO_2-brine mixing. As CO_2 dissolves, the formation brine density increases, resulting in CO_2 saturated brine being approximately 1 - 3 percent denser than original formation water, depending on salinity, P and T (Benson et al. (2005), Ülker et al. (2007)). This density difference will cause instability and, if the reservoir has a high vertical permeability, it may lead to free convection, replacing the CO_2-saturated water from the plume vicinity with unsaturated water, resulting in faster rates of CO_2 dissolution (Benson et al. (2005), Ülker et al. (2007)).

Baines and Worden (2004) reported that the degree to which CO_2 reacts with the formation water, which is dominated by its solubility, will depend on factors such as: pressure, temperature, fluid chemistry, the degree of CO_2-water mixing, or contact surface with CO_2 and water. The extent of these reactions will also depend upon the composition of the rocks and the minerals encountered. According to the authors, formation water chemistry will also be influenced by chemical interaction with the

host formation, meaning that the rates of mineral reactions will also have an impact on CO_2-solubility.

7.1.3 Interaction between CO_2 plume with minerals

Injecting dense CO_2 into saline aquifer could trigger geochemical reactions such as the precipitation of CO_2 with may be beneficial and trap CO_2 in a more permanent state. On the other hand, some reactions may causing mineral dissolution and enhance leakage potential.

According to Benson et al. (2005), geochemical reactions may take several thousand years to have a significant impact on CO_2 sequestration hence it could be neglected during injection phase.

There is evidence that both dissolution and precipitation reactions could occur not just in the reservoir, but in the cap rock as well (Baines and Worden (2004)) Hence it is very important to have a good knowledge of the possible reactions with cap rock when estimating the storage efficiency of a site. The safety of CO_2 sequestration project in the deep sub-surface is very dependent on the type of material constituting the cap rock. One of the most important parameter in CO_2 sequestration project is the pressure. During injection phase the pressure in the CO_2 phase is significantly higher than the CO_2 pressure in natural analogues, hence increasing the capillary breakthrough potential and increase CO_2-solubility in water, which could result in higher reaction rates.

It is important to address both the reactions between dry supercritical CO_2 and the cap rock, and between dissolved CO_2 and the cap rock. If the relatively dry CO_2 is able to contact the cap rock, and if the chemical potential of water in the CO_2 is low enough, it might initiate water loss from the overlying cap rocks, which if extensive, might allow for enhanced CO_2 migration into, or through the cap rock. Dissolved CO_2 may contribute greatly to CO_2 migration. As will be shown later, the reduction of pH as a result of CO_2 dissolution in the brine could result in a decrease in the ability of the

cap rock to prevent CO_2 migration. In addition, dissolution of minerals in the cap rock might result in the formation of flow pathways that might aid CO_2 leakage. The storage safety will be dependent not only on the particular cap rock, e.g. argillites (clays, shales) and evaporites, but also on the minerals constituting the cap rock (e.g. mica or quartz) (Baines and Worden (2004)).

7.2 Alteration of key parameters

Several researches have pointed out the possibility of alteration of both wettability and interfacial tension (IFT) during CO_2 flooding operation. This alteration will obviously change CO_2 threshold pressure to enter a given pore, thus alter the storage capacity of CO_2 (Chiquet et al. (2007b)).

7.2.1 Contact angle alteration

Wettability is very important issue in CO_2 sequestration project. In general, gas is considered as the non-wetting phase. According to Chalbaud et al. (2007a), there is a possibility that injected CO_2 will behave as wetting phase. In strongly water-wet micro models, very thin water films are observed surrounding the solid surface, which become less apparent at increasing pressures. This behavior is due to a reduction in electrostatic interaction which tends to stabilize the water films.

According to Chiquet et al. (2007a), a loss of the water-wettability of the minerals present in cap rocks could decrease or even cancel their capillary-sealing efficiency with respect to CO_2. Such wettability alterations could trigger a high risk to CO_2 underground storage beneath shaly cap rocks, as low CO_2 breakthrough pressures would hence have to be expected.

There are two main factors that affect wettability. First factor is the morphology of the media (e.g. the cap rock), including pore-size distribution, permeability and porosity.

In addition, wettability is also dependent on the chemical composition and particular interactions between the different phases (interfacial tension).

Initially most of the rock sediments are water-wet. In a CO_2/water system, brine will occupy the small pores and form a wetting film on the rock surface which enhances continuity of the wetting phase (Chalbaud et al. 2007b). Wettability will affect CO_2 injectivity and how the displacement proceeds during flooding.

Chiquet et al. (2005) reported that most shale minerals are strongly water-wet in the presence of air and hydrocarbons, but its wettability is altered when CO_2 is in contact with brine in the cap rock. When CO_2 contacts brine, it tends to dissolve into water and forms carbonic acid (H_2CO_3) with a low pH of 3.3 – 3.7. This low pH will tend to alter rock surfaces toward less water wet condition (Rogers and Grieg (2000)). According to Chiquet et al. (2005), such alteration is mainly due to the reduction of electrostatic interactions at the interfaces. These interactions tend to stabilize the brine film and favor water wettability.

Chalbaud et al. (2007b) also observed that the wettability of CO_2 is stronger at low temperature which is due to the increased dissolution of CO_2 hence reducing the electrostatic forces stabilizing the water films.

Chiquet et al. (2007a) performed measurements of contact angle variations with different pressures and mineral surfaces. The contact angle variation that occurs with CO_2 is primarily caused by the change in brine pH that occurs when the pressure is increased, resulting in an increase of the solubility of CO_2 in brine (Chiquet et al. (2007a)).

It can be observed from figures 7.1 and 7.2 that the impact of brine salinity on wettability seems to be limited in the case of quartz, whereas an increase in NaCl concentration seems to reduce the water wettability of mica more strongly. Chiquet et al. (2007a) reported that, at fixed pressures, the contact angle θ_d increased by approximately 25 degrees when the brine salinity was increased from 0.1 to 1 M NaCl. However, the data at 0.01 M NaCl do not obey this trend. This is consistent

with the rather peculiar influence of brine salinity reported by Chiquet et al. (2005). The authors reported that, at fixed pressures, the contact angle decreased by ~20 degrees from 0.01 M NaCl to 0.1 M NaCl, then increased by about the same amount from 0.1 NaCl to 1 M NaCl.

As can be seen from figure 7.1 and 7.2, measurement data is at relatively lower pressure region compared to typical pressure in CO_2 storage. Hence we must extrapolate the data to obtain values for higher pressures.

It is important to understand the trend of the data. Chiquet et al. (2005) presented contact angle alteration curves that more clearly show the trend of these data, and it is evident that a simple linear trend is not sufficient to describe the wettability alteration. In each of the curves, around 50-70 bar, a break in the curve is observed, and each curve can be divided into two linear curves. This break could be a result of the different properties of gaseous CO_2 and supercritical CO_2, as the critical pressure is at 73.82 bar. The spreading of the break-points could be a result of the different salinities in the system.

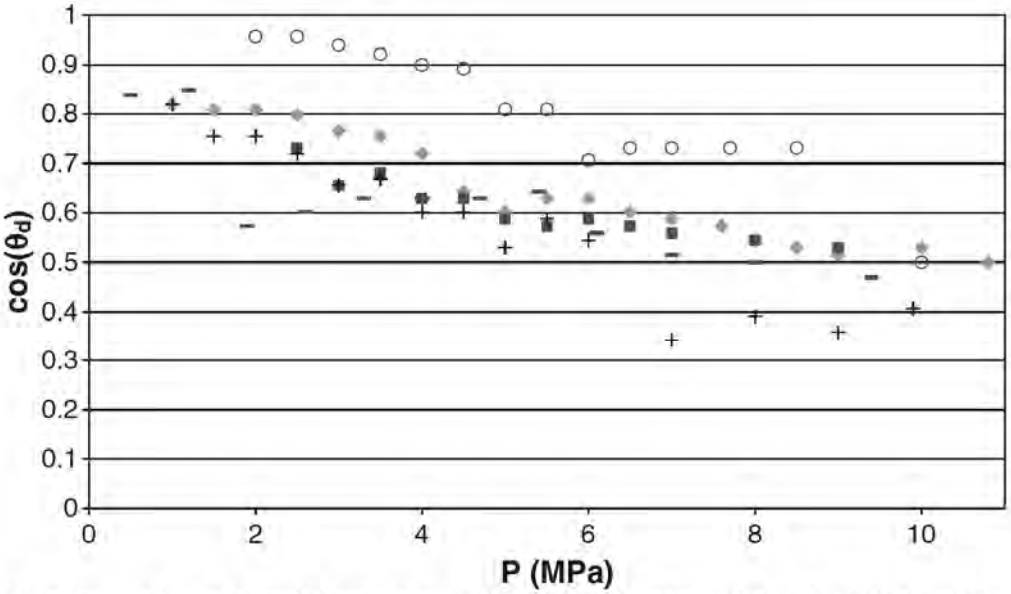

The brines have the following salt (NaCl) contents: 0.01 M (–), 0.1 M (○), 0.2 M (◇), 0.5 M (■) and 1 M NaCl (+).

Figure 7.1: Drainage contact angles on mica as a function of CO_2 pressure. Adapted from Chiquet et al. (2007a).

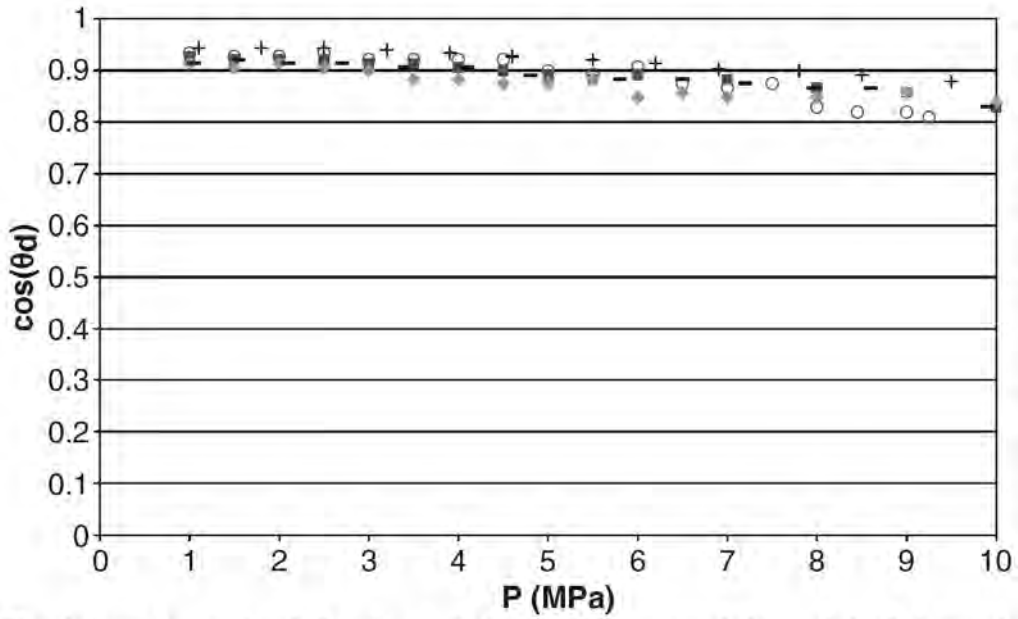

The brines have the following salt (NaCl) contents: 0.01 M (–), 0.1 M (○), 0.2 M (◇), 0.5 M (■) and 1 M NaCl (+).

Figure 7.2: Drainage contact angles on quartz as a function of CO_2 pressure. Adapted from Chiquet et al. (2007a).

Shah et al. (2008) and Tonnet et al. (2008) performed similar experiments with some improvement in the equipment. Shah et al. performed experiments at 35°C up to a CO_2 of 60 bar with low salinity brine (4 g/l NaCl). They observed a similar trend to that observed by Chiquet et al. (2007a) but the effect of pressure to wettability alteration is less pronounced. They also performed experiment on different temperatures (35°C and 75°C) and found that wettability is remains the same within experimental accuracy. On the other hand, they also observed that for quartz, contact angle does not seem to change with pressure.

Experiment results from Tonnet et al. (2008) show that the changes in contact angle with pressure for mica is very moderate. They did not observed any clear trend of wettability alteration due to temperature variation (35°C – 120°C) and brine salinity (low to moderate salinity). In the case of quartz, they obtained similar results with those obtained by Chiquet et al. (2007a).

Summary of experiment results from Chiquet et al. (2007a), Shah et al. (2008) and Tonnet et al. (2008) will be presented in figure 8.1 in this thesis.

7.2.2 Changes in interfacial tension

The storage capacity of CO_2 in a reservoir is very dependent on the maximum CO_2 overpressure that the reservoir seal can sustain, which is dependent on not only the contact angle between the phases, but also on the interfacial tension. It is important to understand how the CO_2/water interfacial tension will behave with varying temperature, pressure and salinity when assessing the efficiency of CO_2 storage in deep geological formations.

According to Chiquet et al. (2007b), at low pressure, the CO_2/brine IFT decreases approximately linearly with increasing pressure and decreasing with increasing temperature.

Above pressures of around 12-15 MPa a pseudo-plateau is reached, showing very limited pressure dependency. The value of this pseudo-plateau decreases with increasing temperature from about 30 mN/m at 308 K to about 23 mN/m at 383 K. This is a temperature trend opposite to that observed for pressures just above about 5 MPa.

The measurements of the CO_2/water system reported by Chiquet et al. (2007b) displayed strong IFT decrease at low pressure, followed by the levelling off in the range of 15-45 MPa. However, no data for pressures over 50 MPa were reported. Rogers and Grigg (2000) reported that interfacial tensions declined asymptotically with increasing temperature and pressure, and the authors supported what Chiquet et al. (2007b) observed; that at higher pressure the IFT is largely independent of pressure. This is according to the authors attributed to the solubility increase of CO_2 in water with pressure. The authors reported that in the proximity (±10-20˚C) of the critical point of CO_2 the IFT decreases rapidly, and a dip in the IFT vs. pressure curve can be observed from figure 7.5. The interfacial tension between the CO_2 water

system is lower than that for water/hydrocarbon systems, and is attributed to the higher miscibility of CO_2 and water versus hydrocarbons and water (Rogers and Grigg (2000)).

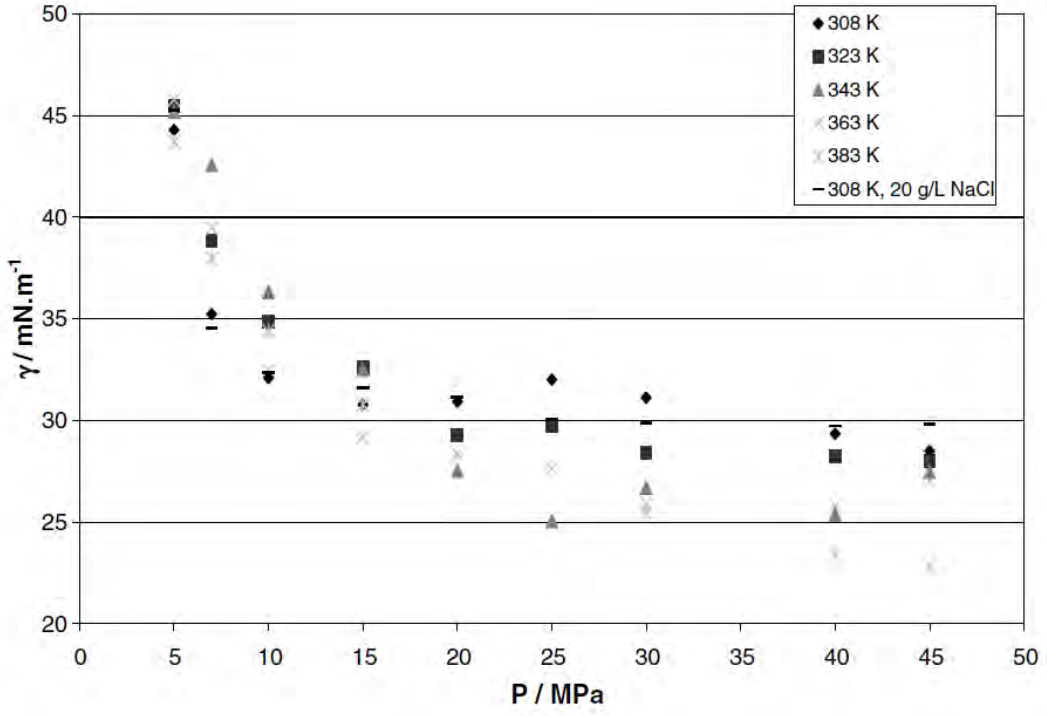

Figure 7.5 Measured isotherms of CO_2/water (or brine) as a function of pressure. Adapted from Chiquet et al. (2007b).

As a rule, the CO_2/brine interfacial tension increases with increasing brine salinity, and the increase is believed to be independent on pressure in the range of 0-6 MPa (Chiquet et al. (2007b)). The authors reported that at a temperature of 298 K, the increase reached about 10 mN/m for the highest salinity investigated, i.e. 5 M NaCl. The increase in IFT with salinity is fairly independent of pressure and reflects the increase in brine surface tension with salinity at ambient pressure, i.e. with no CO_2 present (Chiquet et al. (2007b)). Even though the IFT values for the CO_2/water and CO_2/brine system are about half the CH_4/water IFT values at similar conditions, they still have reasonable values, i.e. above 20 mN/m (Chiquet et al. 2007b).

Interfacial tension will have a large influence on the brine displacement by CO_2, since both the capillary pressure and the relative permeability depend on the interfacial

tension between CO_2 and formation water (brine), but a very strong relationship between computed gas-water ratio (dissolved CO_2) and interfacial tension has also been reported by Bennion and Bachu (2008). The equilibrium IFT between the brine and CO_2 phases is likely to be affected by the amount of dissolved CO_2 at equilibrium conditions, hence by CO_2 solubility.

7.3 Trapping mechanisms

In general, CO_2 trapping mechanism can be categorized into four mechanisms as shown in figure 7.6.

The primary mechanism for trapping CO_2 is through the existence of confining layers or cap rocks such as shale or salt bed that are impermeable to the CO_2. The geometry of the trap takes two dominant forms. The first type of trap is called a structural trapping which is shaped as a dome or anticline, while the second called a stratigraphic trapping derives from lateral variations in the rock type that results in the reservoir layer grading into adjacent confining layers.

As the CO_2 migrates through the pores in the reservoir layer, pockets of CO_2 will adhere to the rock grains, where they will remain due to surface tension effects; this is called residual or capillary trapping,

CO_2 will dissolve in the formation water. CO_2-saturated brine being denser than formation water will sink to the bottom of the reservoir due to buoyancy, hence preventing CO_2 to contact the cap rock. Solubility trapping will be strongly dependent on brine salinity and composition, the density difference between the CO_2 and brine, and permeability and anisotropy (Ülker et al. (2007)).

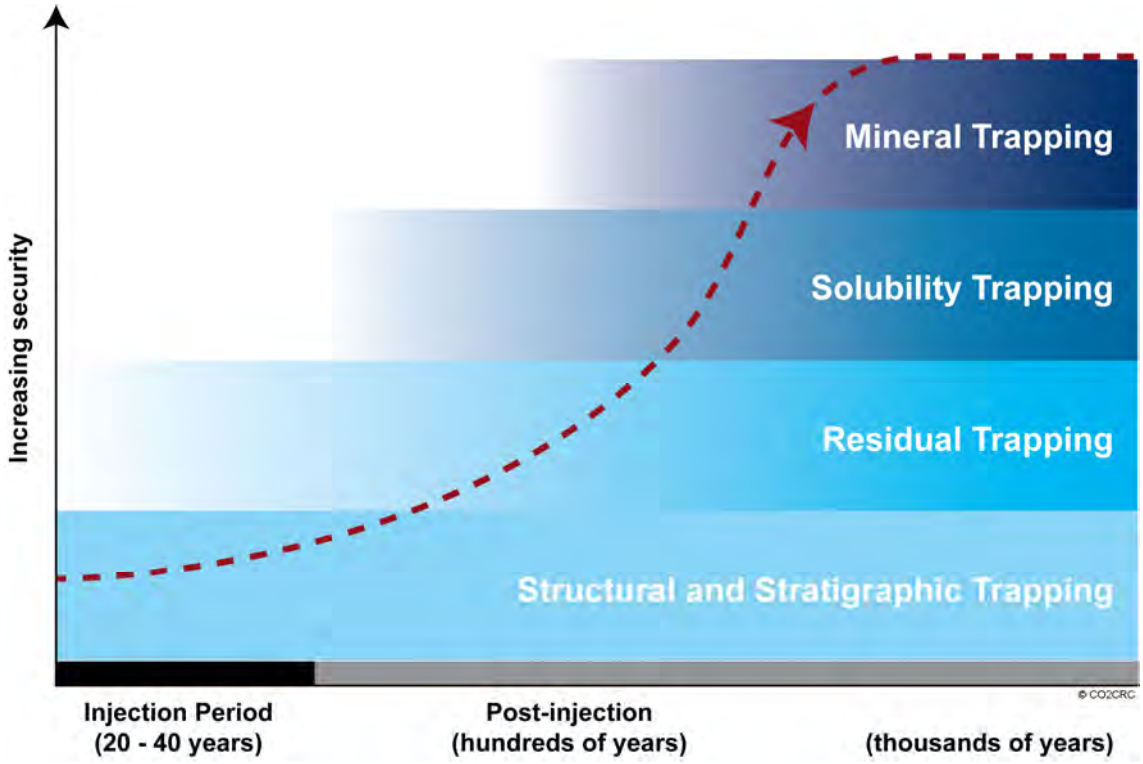

Figure 7.6: Storage security as a function of time, Adapted from The Cooperative Research Centre for Greenhouse Gas Technologies. Adapted from www.co$_2$crc.com.au

Mineral trapping is an important mechanism for the long term storage security of the CO_2 storage project. As previously noted, CO_2 in the underground can undergo a sequence of geochemical interactions with the rock and formation water that will further increase storage capacity and effectiveness. The reactions trapping CO_2 in the form of carbonate minerals are of special interest. Although these reactions are much slower than CO_2-water reactions, they might provide a more permanent sink for CO_2 in the form of carbonate minerals. The stability of carbonate minerals results in CO_2 being effectively immobilized for geological timescales.

8. Summary of main work

8.1 Three-phase flow in porous media

In the first part of this thesis, we are including proper description of three-phase flow in porous media. Three-phase relative permeability has been described by the WAGHYST model from Larsen and Skauge (1998). The model was anchored to observation on laboratory studies and has been used extensively for several WAG simulation models (Kossack (2000), Egermann et al. (2000), Karkooti et al. (2011), Shahverdi et al. (2011)). However, the effect of three-phase capillary pressure was not included in this model, possible due to lack of data. This thesis is partially trying to expand WAGHYST model by including capillary pressure.

Several models have been used to describe three-phase capillary pressure in Eclipse black oil model and other commercial reservoir simulation. The most common technique is Killough hysteresis model (Killough (1976)) which was described earlier in chapter 5. The problem with this technique is that it was solely interpolation of two-phase capillary pressure, hence it depends only on single-phase saturation. However, experiment results from Kalaydjian (1992) and Virnovsky (2004) show that three-phase capillary pressure may depend on saturation of all three-phases.

Another technique is to allow user input three-phase capillary pressure as 2D table where the capillary pressure is a function of saturation for all involved phases. This approach allows more realistic implementation of three-phase capillary pressure in simulation. For Eclipse, this approach is implemented using keyword PCG32D and PCW32D. Unfortunately, Eclipse put a strict rule within these tables in order to be consistent with Killough hysteresis model (Killough (1976)). Three-phase capillary pressure defined using these keywords must be lower than two-phase capillary pressure as illustrated in figure 5.1. Hence, three-phase capillary pressure data from

network model which are consistent with data from Kalaydjian (1992) and Virnovsky (2004), cannot be implemented in ECLIPSE using these keyword.

We have obtained an open source chemical flooding simulation tool from University of Texas Austin. The code is called UTCHEM which was originally coded for chemical flooding simulation. Recently, University of Texas Austin has added three-phase flow simulation into UTCHEM. However, there was not any support for three-phase saturation function. We have implemented both WAGHYST relative permeability model and three-phase capillary pressure table into UTCHEM. Table implementation is slightly relaxed in our implementation compare to Eclipse 100 to accommodate capillary pressure from network model.

WAGHYST relative permeability model in UTCHEM is implemented in a similar way as it is implemented in Eclipse 100. The model requires input of Land's constant, gas relative permeability reduction factor and coefficient for reduction of oil residual saturation due to amount of trapped gas.

Three-phase capillary pressure data are included as two dimension table where oil-water capillary pressure data are function of oil and water saturation. The gas-oil capillary pressure is treated similarly, i.e. the capillary pressures are defined as a function of oil and gas saturation.

It is of great importance to include correct three-phase capillary data into flow simulation. However, these data are not easy to measure since the displacement experiments can follow different saturation paths. Hence it will generally be more difficult experimentally, take longer time and more expensive to obtain these data compared to traditional two-phase flow experiment.

Network model has been investigated as an alternative approach to generate three-phase relative permeability and capillary pressure data (Mani and Mohanty (1998), Fenwick and Blunt (1998), Lerdahl et al. (2000), van Dijke and Sorbie (2002), Piri and Blunt (2005)) Prior to this process, network model is usually anchored to much more available two-phase capillary pressure data.

Initially we tried to anchor network model manually, trying out several combinations of parameters and check which combination give the best fit. Unfortunately, with the numerous amount of parameters involved, it is not feasible to use this approach. As an example, evaluating each of these parameters at minimum, median and maximum values will need 3^n number of network simulation with n represent number of parameters. Evidently, the number of network simulation will grow exponentially with number of parameters. In addition, the process can be complicated further since some of the parameters are strongly related to other parameters such as minimum and maximum radius.

In this thesis, we have explored the possibility of implementing experimental design and ensemble Kalman Filter technique as a tool for automating capillary pressure matching process. Details on implementation of these methods are presented in chapter 4 and publication 2.

We run a synthetic network model to generate capillary pressure for primary drainage and imbibition process (with aging process) and use the capillary pressure as our matching target. We also add noise (maximum 10%) into capillary pressure data in order to mimic experiment data. The parameters for both techniques were initialized with the same range. Both techniques were started with the same parameter range. We run 100 network simulations for each matching process and update the model accordingly afterward.

Our trial on synthetic network mode shows that ensemble Kalman Filter converged faster and matched solution more accurate compared to experimental design. We believe this is due to sampling technique in ensemble Kalman Filter which spreads along the parameter range. Experimental design, on the other hand, only used three values for each parameter which minimum, median and maximum values. Hence the technique might fail to locate global solution value for the parameters, especially when parameters are widely spread.

Another issue with experimental design is that sometimes RSM model gives a wrong direction of parameter shifting. This could be due to interaction between parameters that is not modeled properly into RSM model. The problem could become critical since we shrunk parameters range every time we update the model based on indication from RSM model. Experimental design cannot recover from this error since the solution will be outside of the range after updating. Ensemble Kalman Filter does not have this limitation since the parameter ranges are kept constant so that the method can correct any misdirection at each step. In addition, there is no need to model the interaction between parameters as it is checked statistically in ensemble Kalman Filter method.

Anchored network model can then be used to generate three-phase capillary pressure. We performed full primary drainage process, followed by imbibition process on anchored network model. Imbibition process is stopped at different saturation level and followed by full secondary drainage process. Due to complexity of the process involved, network model assumed constant capillary pressure between two non-displacing fluids during secondary drainage. For example, in gas injection process after water injection, network model will assume that oil-water capillary pressure remains constant for the whole secondary drainage process. The value for this oil-water capillary pressure during this process is taking from last oil-water capillary pressure during imbibition process. This assumption is not necessarily correct but it is important to establish so that network model can calculate the other capillary pressure.

Three-phase capillary pressure from network model are collected for different initial saturation level and smoothed as a surface in MATLAB. The smoothing process is important for reservoir simulation as it will reduce instability due to non-continuous capillary pressure derivation. The best approach to include this surface into UTCHEM is to have an analytic equation that smooth three-phase capillary pressure surfaces and implement it into UTCHEM. However, due to the complexity of the surface, it is difficult to fit it into one analytic equation. As an alternative, we have put a detailed

three-phase capillary pressure with saturation step for both phases smaller than 0.01 fraction. We have observed that larger three-phase capillary pressure table improves the stability of simulation and allow faster simulation process.

In order to keep consistency of saturation end-point between relative permeability and capillary pressure, we have stretched three-phase capillary pressure to cover the same end-point as in two-phase flow. Hence it will cover the domain where relative permeability is covering.

As mentioned earlier, we have modified UTCHEM to include three-phase flow description. In order to verify its accuracy, we have performed simulations of several synthetic cases on both Eclipse 100 and UTCHEM. We have used both zero capillary pressure and two-phase capillary pressure in all cases as Eclipse has limited implementation of three-phase capillary pressure. For both cases, we used WAGHYST model to represent three-phase relative permeability. In general, we see a similar result from both simulators. There are some small discrepancy between cases but they are in a negligible amount which is probably due to different solver implementation in the simulator.

Three-phase flow simulation results without capillary pressure were compared to the cases with two-phase capillary pressure. The observation shows that the differences are negligible for any wettability condition as reported in publication 3. It is important to understand that this observation is very dependent on the scale of the model. In the field scale, the effect of capillary force is usually much lower compare to viscous force, hence the effect of capillary pressure in this scale is usually negligible. Dale and Skauge (2007) perform simulation study in core scale and show that oil recovery is strongly affected by two-phase capillary pressure.

Including three-phase capillary pressure seems to affect oil recovery efficiency significantly even at field scale simulation. The effect is very dependent on wettability of the rock as three-phase capillary pressure surfaces are mainly related to the rock wettability.

In publication 3, we generated three-phase capillary pressure for different rock wettability and perform flooding simulation. We saw that maximum oil recovery is attained in the scenario where gas injection is followed by water flooding (G1W2 process) in rock with strongly water-wet condition. This simulation result is in accordance with observation by Skauge (1994). Another important observation is that G1W2 process will attain the higher recovery efficiency compared to W1G2 process (water injection followed by gas injection) regardless of rock wettability in our studies (strongly water-wet, strongly oil-wet and intermediate-wet)

For all kind of rock-wettability system, including three-phase capillary pressure significantly increase oil recovery efficiency for W1G2 process and reduce oil recovery efficiency for G1W2 process. The effect of three-phase capillary pressure is most significant for strongly water-wet case with G1W2 process and strongly oil-wet case with W1G2 process.

8.2 Wettability alteration during CO_2 sequestration

Several researchers have pointed out that wetting preference of a mineral could change when being contacted by carbonic acid (Chalbaud et al. (2007a), Chiquet et al. (2005), Chiquet et al. (2007a), Shah et al. (2008), Tonnet et al. (2008)). The resulting reduction in pH toward the iso-electric point of the mineral will tend to reduce the water wettability towards a state of more intermediate wetting.

In order to investigate the effect of wettability alteration during CO_2 sequestration, we have built a representative model of Johansen formation, a candidate for CO_2 sequestration project.

In addition, we have also performed sensitivity studies on several parameters that are considered crucial for storage capacity such as solubility effect, diffusion effect, variations in injection rate, permeability anisotropy for both reservoir and cap rock, and porosity effect.

Base on simulation result for Johansen model, we found that diffusion has a large effect on storage capacity of the cap rock, second to wettability alteration. Diffusion acted as another migration mechanism and migrate CO_2 from higher concentration zone to low concentration zone i.e. cap rock. Including diffusion into simulation allows CO_2 migrated toward cap rock and increases the potential of leakage. Laboratory experiments show that diffusion coefficient is increasing with temperature (Tamimi et al. (1994)). The diffusion coefficient increases more at higher temperature, indicating that it is important to choose storage location with lower temperature. In general, rock temperature increase at deeper formation with a relatively constant rate. The geothermal gradient is varied with location. In most of the places which is away from tectonic plate, geothermal gradient is range between 25-30^{o}C per km. Hence it is preferred to have a shallow injection point in this case to lessen CO_2 migration due to diffusion.

Another important parameter to consider is CO_2 solubility into water. Water is capable of capturing large amount of CO_2. The solubility is dependent on pressure, temperature and salinity as described in chapter 6. Simulation study excluding CO_2 solubility shows large amount of free gas accumulated underneath the cap rock and consequently increase the potential of leakage. Hence it is necessary to consider this mechanism when we choose injection location.

Hysteresis contributes a significant portion of trapping CO_2 into porous media. This mechanism started to take into account when injection is stopped and water imbibed CO_2. As water is the wetting phase, CO_2 might be trapped inside the pore as described in chapter 3. Simulation results show that including hysteresis into simulation leads to a lower CO_2 accumulation underneath the cap rock as some of them are trapped within reservoir.

Sensitivity study on petrophysical properties of both shale and reservoir shows a small effect of these properties on CO_2 sequestration safety. The most important petrophysical property is shale anisotropy. Higher anisotropy value means higher

vertical permeability which leads to more vertical migration from reservoir to cap rock, thus increase the risk of CO_2 leak to surface.

As the focus of this study is wettability alteration, we have collected several measured wettability alteration experiment results due to CO_2 injection. These experiment data show a decreasing contact angle between gas and water, hence reduce the water-wet state of the rock as CO_2 pressure is increasing. However, these experiments show a very different values for mica (figure 8.1) while quartz experiment results (figure 8.2) show a very good agreement.

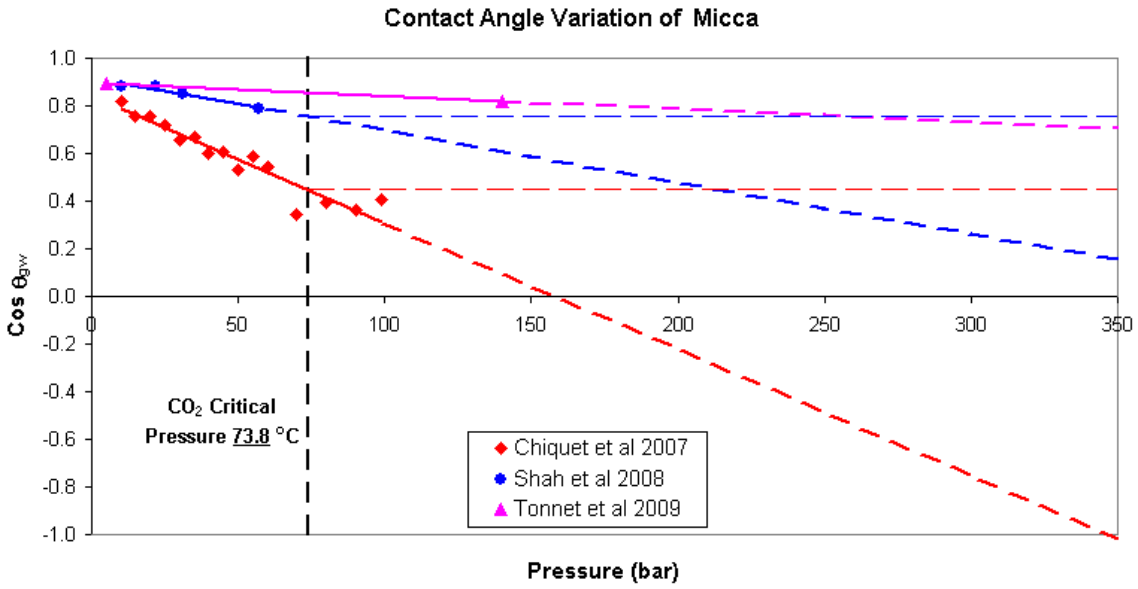

Figure 8.1: Contact angle alteration for mica based on experiment from Chiquet et al. (2007a), Shah et al. (2008) and Tonnet et al. (2008)

In this study, we assume that shale layer is assumed to contain pure mica and reservoir (sand) contains pure quartz. We understand that in reality, the layers can contain both mica and quartz and some other minerals as well. However, there are limited experiment data on wettability alteration and they only perform experiment on typical mineral such as quart and mica.

Experiment data were performed at relatively low pressure which is probably due to pressure constraint of experiment equipment. We only have information for pressure lower than 150 bar. In the case for Johansen formation, the reservoir will be exposed

to high pressure, up to maximum of 350 bar due to formation depth. As a consequence, we need to extrapolate experiment data far away from available data. The most logical choice would be to perform linear extrapolation since we did not see any strong trend of other correlation. We realized that extrapolation give an large uncertainty hence we added more sensitivity where we assumed that wettability alteration is stopped when CO_2 has reached critical pressure and CO_2 will maintain the same wettability from this critical pressure. We assume that the representative wettability alteration process should lies between these two cases. We did not perform extra case for experimental result from Tonnet et al. (2008) as there are only two data points and one of them has exceeded critical pressure.

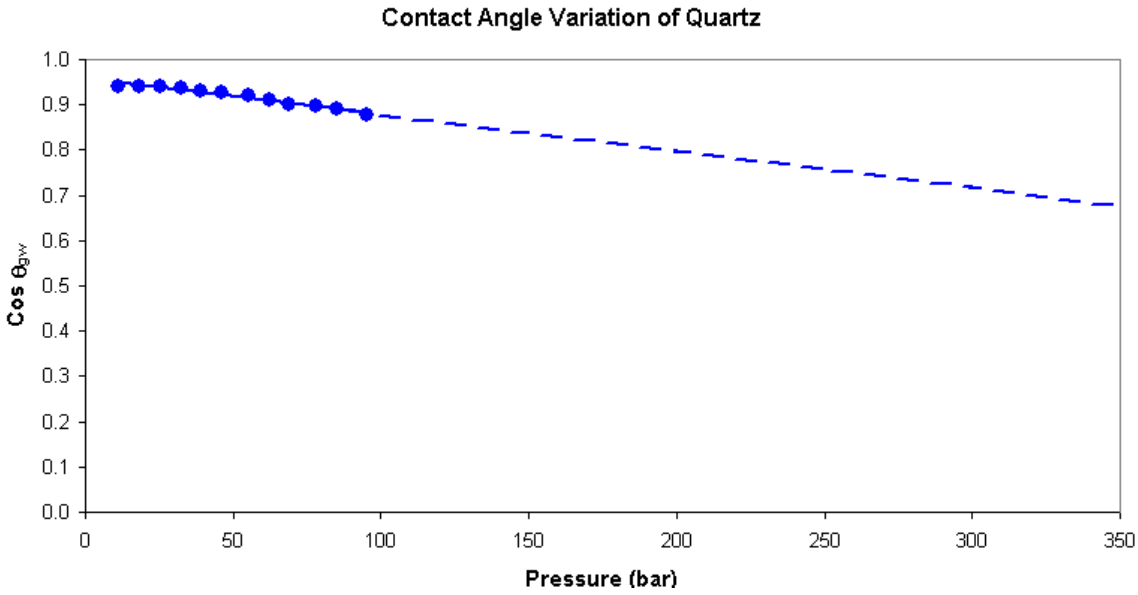

Figure 8.2: Contact angle alteration for quartz based on experiment data from Chiquet et al. (2007a)

In most commercial simulator, there is no option for wettability alteration. This is the case with GEM-GHG simulator that we use in this study. GEM-GHG is a commercial compositional simulator that has a detail model on CO_2 sequestration. Due to the lack of wettability alteration option in the simulator, we have to perform a semi-dynamic simulation study. We prepared several sets of saturation functions which were generated from network model for different wettability condition. Each set of saturation function is valid on certain range of block pressure. The simulation is then

run for 10 years and then stopped, grid blocks pressure and CO_2 saturation are reported at the end of this 10 years period. Based on pressure and CO_2 saturation at each grid block, we assign new saturation function in that particular grid block. The simulation is then run for another 10 years period. The sequence is repeated until the end of injection period. We also performed wettability alteration after injection period. We have chosen longer time period i.e. 50 years period as we expect less migration process after injection is stopped.

Reduction in wettability of the storage layer strongly affects both the migration of CO_2 into the cap rock, and especially the migration of CO_2 within the formation. We observe that wettability alteration will reduce the amount of CO_2 distributed in sand layer. A large portion of CO_2 migrated into shale layer as shown clearly in alteration at the end of injection period.

The scenario where wettability alteration is stopped at pressure above critical pressure shows more leakage potential for alteration data based on Chiquet et al. (2007a). This is probably due to higher gas relative permeability for this particular case. This observation is interesting considering that this particular case is neither the worst or the best scenario for wettability alteration. Hence, proper simulation study must be performed to evaluate the safety of CO_2 sequestration on a given wettability alteration potential.

Simulation study for Johansen formation shows an interesting result. Some of the mechanisms can affect the other migration mechanisms. For example, diffusion can assist migration of CO_2 hence rock will have its wettability altered thus lower CO_2 capillary entrance pressure of that particular grid block. We have performed simulation study focusing on the effect of wettability alteration with other migration mechanisms. In this simulation study, wettability alteration was based on experiment data from Tonnet et al. (2008) which is the recent experiment data.

Including diffusion in the simulation leads to increase amount of CO_2 in cap rock. This result is in accordance with simulation study for Johansen formation. However,

the case which includes both diffusion and wettability alteration shows lower amount of CO_2 in cap rock. Possible explanation is that combining both diffusion and wettability alteration leads to more severe wettability alteration. Although capillary pressure is reduced greatly, CO_2 does not migrate into cap rock easily since relative permeability is reduced as well.

Heterogeneity in this study is modeled based on Dykstra-Parsons coefficient. Simulation study with heterogeneity variation in both sand and shale layers shows a negligible effect on amount of CO_2 in cap rock. However, after including wettability alteration in the simulation, we noticed significant changes for different heterogeneity. A significant reduction of CO_2 amount in cap rock was encountered for sand Dykstra-Parsons coefficient higher than 0.4. This is probably due to the existence of low permeability barrier at high Dykstra-Parsons coefficient. The barriers will tend to reduce vertical migration more that lateral one as we have chosen anisotropy ratio value of 0.1.

Similar observation was seen for sensitivity in shale heterogeneity. Lower amount of CO_2 in cap rock at higher heterogeneity were due to existence of flow barrier. However the impact is not as large as sand heterogeneity variation. The reason for such observation is that most of migration is taking place in sand layers. Shale barrier will only contribute at later stage of simulation.

Ideally, rock wettability is altered spontaneous when rock surface is in contact with CO_2. However, due to limitation of simulator, we need to perform wettability alteration in a semi-dynamic way. Alteration at smaller time step will require a large effort to perform since it involves a lot of manual work. Hence it is interesting to see the impact of wettability alteration frequency. Our simulation study shows that increasing the frequency of wettability alteration 5 times can increase the amount of CO_2 in cap rock by 4 times. Reducing the frequency also shows a reduction in the leakage risk. Despite of the high impact of wettability alteration frequency, it is not feasible to perform such alteration with high frequency manually. Hence it is

recommended to modify the simulator to allow for wettability alteration within the simulator itself.

Grid dimension is an important issue in simulation. Smaller grid block size is recommended to reduce numerical dispersion. However, it will increase simulation time significantly. Hence we need to find balance between these two factors. For this study, we refine grid size by a factor of two at each direction. In addition, refinement by factor of two in all direction was also performed. Grid block permeability is distributed prior to refinement hence there is not any effect of random permeability distribution. Significant increase in leakage risk were seen for grid refinement in one direction i.e. refinement in lateral direction or vertical direction only. However, it is interesting to mention that leakage risk is reduced even more that base case in the case where refinement were done in both direction. Possible explanation is one direction refinement enhance CO_2 vertical migration.

It is important to note that these observations are dependent on the choice of wettability alteration model. The effect of reduced wettability is dependent on the balance between decrease in capillary pressure entrance and decrease in gas and water relative permeability.

9. Concluding Remarks

9.1 Three-phase flow in porous media

Three-phase relative permeability and capillary pressure have been included into UTCHEM simulator. This will allow proper modeling of three-phase flow in porous media. Three-phase relative permeability model is based on WAGHYST model from Larsen and Skauge (1998). Three-phase capillary pressure surfaces are generated from network model. The simulator code is calibrated against Eclipse reservoir simulator and gave good match.

Three-phase capillary pressure can be generated from network model that is anchored to two-phase experiment data. We have implemented both experimental design and ensemble Kalman-Filter as a tool for automatic capillary pressure matching. From our trial with a synthetic network model, we saw that ensemble Kalman-Filter is superior compared to experimental design.

Three-phase capillary pressure generated from network model shows that absolute maximum three-phase capillary pressure is higher than two-phase capillary pressure. This is mainly the reason that three-phase capillary pressure has significant effect compared to two-phase capillary pressure.

Including three-phase capillary pressure will increase oil recovery especially for W1G2 process while it will reduce recovery for the G1W2 process. Three-phase capillary pressure has the most influence in strongly water-wet cases for G1W2 and strongly oil-wet cases for the W1G2 process.

9.2 Wettability alteration during CO_2 sequestration

Simulation study on CO_2 sequestration shows that migration of CO_2 is strongly dependent on the heterogeneity of the aquifer, an important controller of fluid flow, especially on the Norwegian Continental Shelf. Including the solubility effects has shown a large influence on the CO_2-water displacement, considering that a larger amount of CO_2 accumulates underneath the cap rock when dissolution is ignored. Low permeability anisotropy is preferred for ideal storage location as it will act as barrier preventing CO_2 upward migration.

Hysteresis plays an important role in CO_2 sequestration project after injection ended and water starts to imbibe into pore filled with gas. Water will displace gas and some of the gas will be trapped in the pore.

In general, diffusion will increase the risk of leakage and enhance wettability alteration. However, in some cases, due to lower gas relative permeability as wettability is reduced, the safety of CO_2 sequestration can be enhanced.

Heterogeneity of both sand and shale layers has inverse relationship with amount of CO_2 migrate to cap rock.

The frequency of wettability alteration can influence the risk assessment. Simulation study shows that increasing the frequency of wettability alteration will increase the amount of CO_2 migrate to cap rock. However, it is often impractical to perform wettability alteration too frequent hence the right balance is needed.

10. Further work

During the work on this thesis, several issues have emerged that would benefit for further investigation.

Convergence of experimental design can be enhanced by changing the algorithm for solution finding. Instead of bisection method, we can perform simulation at more points on important parameters and the best solution can be picked up for further iteration process. In addition, it is interesting to see how RSM model behave if we include interaction between parameters.

Automatic history matching of two-phase capillary pressure can be optimized further combining both experimental design and ensemble Kalman-filter. Experimental design can be employed to select significant parameters and ensemble Kalman-Filter are then used to find solution value on these significant parameters. Using such technique, there will be less noise from insignificant parameters that need to evaluate using ensemble Kalman-filter method hence it could increase convergence rate.

Simulation will benefit from smooth capillary pressure representation. Three-phase capillary pressure will need to be smooth against analytical equation. More advance study can be performed to model capillary pressure hysteresis based on this analytical equation. However, consistent end-point saturation need to be carefully treated as process is changing so that end-point saturation might be shifted at each process.

Another issue that is worth to pursue is the impact of constant capillary pressure assumption when performing secondary drainage process. Network model can be modified to calculate three-phase capillary pressure when capillary pressure of three pairs of fluids is changing.

CO_2 sequestration study can be extended to incorporate the effect of geochemistry reaction in the storage to wettability alteration. Some geochemistry reactions change the pH level of the system which can trigger wettability alteration of the rock.

Reservoir simulator can be stopped for each certain duration, checked for pH level on each block and altered saturation function according to its pH condition.

It is also interesting to see severity of wettability alteration on mixed mineral composition. However, since there is not any published experiment result on mixed mineral, it is perhaps easier to model the process mathematically.

References

1. Abdallah, W., Zhao, W., Gmira, A., (2011) Sensitivity Analysis of Interfacial Tension on Saturation and Relative Permeability Model Predictions, SPE 149038

2. Akervoll, I., Bergmo, P.E.S. (2009) A Study of Johansen Formation Located Offshore Mongstad as a Candidate for Permanent CO_2 Storage, SINTEF Petroleum Research, Trondheim, Norway.

3. Al-Bazali, T.M., Zhang, J., Chenevert, M.E., Sharma, M.M. (2009) An Experimental Investigation of Capillary Pressure, Diffusion, Osmosis, and Chemical Osmosis on the Stability and Reservoir Hydrocarbon Capacity of Shales, SPE 121451.

4. Angeli, M., Soldal, M., Skurtveit, E., Aker, E. (2009) Experimental percolation of supercritical CO_2 through a caprock. ScienceDirect, Energy Procedia 1 (2009), 3351-3358.

5. Baines, S.J., Worden, R.H. (2004) Geological storage of carbon dioxide. Geological Society Special publication 233. 87-103.

6. Bardon, C., Longeron, D.G., (1980) Influence of Very Low Interfacial Tensions on Relative Permeability, SPE 7609

7. Bartell, F.E., Osterhof, H.J. (1927) Determination of the Wettability of a Solid by a Liquid, Ind. Eng. Chem. 19, 1277-1280.

8. Bennion, D.B., Bachu, S. (2008) A Correlation of the Interfacial Tension between Supercritical Phase CO_2 and Equilibrium Brines as a Function of Salinity, Temperature and Pressure. SPE Annual Technical Conference and Exhibition, Denver, Colorado, USA, 21-24 September 2008.SPE 114479. 1-4.

9. Benson, S., Cook, P., etc (2005), Chapter 5. Underground geological storage, IPCC Special report, Carbon dixoide capture and storage, 195-276.

10. Benson, S.M. (2006) Monitoring Carbon Dioxide Sequestration in Deep Geological Formations for Inventory Verification and Carbon Credits. SPE Annual Technical Conference and Exhibition, San Antonio, Texas, USA, 24-27 September 2006. SPE 102833. 1-14.

11. Bergmo, P.E.S, Lindeberg, E., Riis, F., Johansen, W.T. (2009) Exploring geological storage sites for CO_2 from Norwegian gas power plants: Johansen formation. Energy Procedia Volume 1, Issue 1, 2945-2952.

12. Brooks, R. H. and Corey, A. T. (1966) Properties of Porous Media Affecting Fluid Flow, J. Irrig. Drain. Div.

13. Bryant, S.L., Lakshminarasimhan, S., Pope, G.A. (2006) Buoyancy-Dominated Multiphase Flow and its Impact on Geological Sequestration of CO_2. Symposium on Improved Oil Recovery, Tulsa Oklahoma USA 2006, SPE 99938.

14. Buckley, J. S. (1996) Mechanisms and consequences of wettability alteration by crude oils, Department of Petroleum Engineering, Heriot-Watt university

15. Buckley, J. S., Fan, T. (2005) Crude Oil/Brine Interfacial Tensions, SCA2005-01, presented at the International Symposium of the Society of Core Analyst, Toronto, Canada

16. Bøe, R., Magnus, C., Osmundsen, P.T., Rinstad, B.I. (2002) CO_2 point sources and subsurface storage capacities for CO_2 in aquifers in Norway. NGU Report 2002.

17. Carlson, F. M., (1981) Simulation of relative permeability hysteresis to the non-wetting phase, presented at the 56th annual technical conference and exhibition, San Antonio, SPE 10157

18. Chalbaud, C., Robin, M., Bekri, S., Egermann, P. (2007a) Wettability Impact on CO_2 Storage in Aquifers: Visualisation and Quantification using Micromodel Tests, Pore Network Model and Reservoir Simulations. International Symposium of Core Analysts, Calgary, Canada, 10-12 September, 2007. 1-12.

19. Chalbaud, C., Lombard, J.M., Martin, F., Robin, M., Bertin, H., Egermann, P. (2007b) Two Phase Flow Properties of Brine-CO_2 Systems in Carbonate Core: Influence of Wettability on Pc and kr. SPE 111420.

20. Chiquet, P., Broseta, D., Thibeau, S. (2005) Capillary Alteration of Shaly Cap rocks by Carbon Dioxide. SPE Europe/EAGE Annual Conference, Madrid, Spain, 13-16 June 2005. SPE 94183. 1-10.

21. Chiquet, P., Broseta, D., Thibeah, S. (2007a) Wettability alteration of cap rock minerals by carbon dioxide. Geofluids. 112-122.

22. Chiquet, P., Darion, J-L., Broseta, D., Thibeau, S. (2007b) CO_2/water interfacial tensions under pressure and temperature conditions of CO_2 geological storage. ScienceDirect, Energy Conversion and Management 48 (2007). 736-744.

23. Christensen, J.R., Stenby, E.H., and Skauge, A. (2001) Review of WAG field experience. SPE 71203, SPERE &E Journal, 97-106

24. Corey, A. T. (1954) The interrelation between gas and oil relative permeabilities, Prod. Mon., pp. 19, 38

25. Dale, E. I., and Skauge, A. (2005) Fluid flow properties of WAG injection processes. 13th European Symposium on Improved Oil Recovery, Budapest, Hungary

26. Dale, E. I., and Skauge, A. (2007) Features concerning capillary pressure and the effect on the two-phase and three-phase flow. 14th European Symposium on Improved Oil Recovery, Cairo.

27. Daniel, R.F., Kaldi, J.G. (2008) Evaluating seal capacity of caprocks and intraformational barriers for the geosequestration of CO_2. PESA Eastern Australian Basins Synposium 2, 475-483.

28. Drummond, C., Israelachvili, J. (2002) Surface forces and wettability. ScienceDirect, Journal of Petroleum Science and Engineering 33 (2002). 123-133.

29. Eclipse Technical Description 2008, Schlumberger

30. Egermann, P., Vizika, O., Dallet, L., Requin, C., Sonier, F. (2000) Hysteresis in Three-Phase Flow: Experiments, Modeling and Reservoir Simulations, SPE 65127

31. Eigestad, G.T., Dahle, H.K., Hellevang, B., Riis, F., Johansen, W.T. Øian, E. (2009) Geological modelling and simulation of CO_2 injection in the Johansen Formation.

32. Ennis-king, J., Paterson, L. (2005) Role of convective mixing in the long-term storage of carbon dioxide in deep saline formations, SPE 84344

33. Fenwick, D. H., and Blunt, M. J., (1998) Network modelling of three-phase flow in porous media, SPEJ3(1), pp. 86-97

34. Freund, P., Adegbulugbe, A., Christophersen, Ø., Ishaitani, H., Moomaw, W., Moreira, J. (2005a) Carbon dioxide capture and storage, 1 Introduction, IPCC Special report, Carbon dixode capture and storage 53-72.

35. Freund, P., Bachu, S., Simbec, D., Thambimuthu, K., Gupta, M. (2005b) Annex 1, Properties of CO_2 and carbon-based fuels, IPCC Special report, Carbon dioxide capture and storage

36. GEM user guide. (2008) Advanced compositional reservoir simulator. computer modelling group Ltd.

37. Hawes, R.I., Dawe, R.A., Evans, R.N., Grattoni, C.A. (1996) The depressurization of water-flooded reservoirs; wettability and critical gas saturation. Petroleum Geoscience; May 1996; v. 2; no. 2; 117-123.

38. Helland, J. O., Skjæveland, S. M. (2004) Three-phase capillary pressure correlation for mixed-wet reservoir, Proceeding SPE internation petroleum conference in Mexico, SPE 92057

39. Hirasaki, G.J. (1991) Wettability: Fundamentals and Surface Forces. SPE, Shell Development CO. SPE Formation Evaluation, June 1991.

40. Holm, R., Kaufmann, R., Dale, E.I., Aanonsen, S., Fladmark, G.E., Espedal, M., Skauge, A. (2009) Constructing Three-Phase Capillary Pressure Functions by Parameter Matching Using a Modified Ensemble Kalman filter, Communication in Computational Physics

41. Holmgren, C. R. and Morse, R. A. (1951) Effect of Free Gas Saturation on Oil Recovery by Water Flooding. Pet. Trans. AIME 192, 135-140.

42. Imbus, S., ORR, F.M., Kuuskra, V.A., Kheshgi, H., Bennaceur, K., Gupta, N., Rigg, A., Hovorka, S., Myer, L., Benson, S. (2006) Critical issues in CO_2 capture and storage: Findings of the SPE Advanced Technology Workshop (ATW) on Carbon Sequestration. SPE Annual Technical Conference and Exhibition, San Antonio, Texas, USA, 24-27 September 2006, SPE 102968. 1-7.

43. Jerauld, G.R., Saltier, S.J. (1990) The effect of pore-structure on hysteresis in relative permeability and capillary pressure: pore-level modeling. Transport in Porous Media 5, 103-151.

44. Johnson, J.W., Nitao, J.J., Steefel, C.I. & Knauss, K.G. (2001) Reactive transport modelling of geologic CO_2 sequestration in saline aquifers: The influence of intra-aquifer shales and the relative effectiveness of structural, solubility, and mineral trapping during prograde and retrograde sequestration. Procedings of the First National Conference of Carbon Sequestration, Washington, DC, May 14-17, 2001.

45. Juanes, R., Spiteri, E.J., ORR, F.M.Jr., Blunt, M.J. (2006) Impact of relative permeability hysteresis on geological CO_2 storage. Water resources research, vol. 42, 2006.

46. Kalaydjian F. (1992) Performance and analysis of three-phase capillary pressure curves for drainage and imbibition in porous media, SPE ATCE (vol Reservoir Engineering), Washington DC

47. Karkooti, H., Masoudi, R., Arif, A.M., Darman, N.H., Othman, M.B. (2011) Evaluation of the Impact of Relative Permeability Hysteresis and Three Phase Modeling on the Performance of Water Alternative Gas EOR Processes, SPE 143982

48. Khaled, G.A.M., Dickson, K.B., Shaver, R.D., Robinson Jr., R.L (1993) Experimental Phase Densities and Interfacial Tension for a CO_2/Synthetic-Oil and a CO_2/Reservoir-Oil system. SPE 22216

49. Killough, J. E. (1976) Reservoir simulation with history-dependent saturation functions, Trans. AIME 261, pp. 37-48.

50. Kortekaas, T.F.M. and van Poelgeest, F (1991) Liberation of solution gas during pressure depletion of virgin and watered-out oil resevoirs, SPERE 329-335.

51. Kossack, C.A. (2000) Comparison of Reservoir Simulation Hysteresis Options, SPE 63147.

52. Kralik, J. G., Manak, L. J., Jerauld, G. R. and Spence, S. P. (2000) Effect of Trapped Gas on Relative Permeability and Residual Oil Saturation in Oil-Wet Sandstone., 75th ATCE symposium, Dallas. SPE 62997

53. Kumar, S., Torabzadeh, S.J., Handy, L.L. (1985) Relative Permeability Functions for High- and Low-Tension Systems at Elevated Temperatures, SPE 13670

54. Kyte, J. R., Stanclift, R. J. Jr., Stephan, S. C. Jr. and Rapoport L. A. (1956) Mechanism of Water Flooding in the Presence of Free Gas, Pet. Trans. AIME 207, 215-221.

55. Lam, C.N.C., Wu, R., LI, D., Hair, M.L, Neumann, A.W. (2002) Study of the advancing and receding contact angles: liquid sorption as a cause of contact angle hysteresis. Advances in Colloid and Interfacial Science 96, 169-191.

56. Larsen, J. A., and Skauge, A. (1998) Methodology for Numerical Simulation with Cycle-Dependent Relative Permeabilities, Society of Petroleum Engineers Journal, 163-73.

57. Lerdahl, T.R., Øren, P.E., Bakke, S. (2000) A Predictive Network Model for Three-Phase Flow in Porous Media, SPE 59311

58. Livingston, H.K. (1938) Surface and Interfacial Tension of Oil-Water Systems in Texas Oil Sands, Journal of Petroleum Technology

59. Lomeland, F., Ebeltoft, E., Thomas, W. H., (2005) A new versatile relative permeability correlation, reviewed proceedings of the International Symposium of the Society of Core Analysts held in Toronto, Canada.

60. Ma, T. D. and Youngren, G. K. (1994) Performance of Immiscible Water-Alternating-Gas (IWAG) injection at Kuparuk River Unit, North Slope, Alaska, SPE 28602, 69th ATCE symposium, New Orleans

61. Mani, V., and Mohanty, K. K. (1998) Pore-level network modeling of three-phase capillary pressure and relative permeability curves, SPEJ 3, pp. 337-353

62. McCaffery, F.G. (1972) Measurement of Interfacial Tensions and Contact Angles at High Temperature and Pressure, Journal of Canadian Petroleum Technology

63. Mungan, N (1964) Role of Wettability and Interfacial Tension in Water Flooding, SPE 705

64. Mo, S., Akervoll, I. (2005) Modeling long-term CO_2 storage in aquifer with a black-oil reservoir simulator. 2005 SPE/EPA/DOE Exploration and Production Environmental Conference held in Galveston, Texas, U.S.A.

65. Nelson, P.H. (2009) Pore-throat sizes in sandstones, tight sandstones, and shales. AAPG Bulletin, V. 93, NO. 3 (March 2009), 329-340.

66. Okasha, T.M., Al-Shiwaish, A.A. (2009) Effect of Brine Salinity on Interfacial Tension in Arab-D Carbonate Reservoir, Saudi Arabia, SPE 119600.

67. Okasha, T.M., Al-Shiwaish, A.A. (2010) Effect of Temperature and Pressure on Interfacial Tension and Contact Angle of Khuff Gas Reservoir, Saudi Arabia, SPE 136934.

68. Qi, R., Beraldo, V., LaForce, T., Blunt, M.J. (2007) Design of Carbon Dioxide Storage in a North Sea Aquifer Using Streamline-Based Simulation. SPE Annual Technical Conference and Exhibition , Anaheim, California, USA, SPE 109905. 1-7.

69. Piri, M., and Blunt, M. J. (2005) Three-dimensional mixed-wet pore-scale network modeling of two- and three-phase flow in porous media, Phys. Rev. E. 71, 026302.

70. Rogers, J.D., Grigg, R.B. (2000) A literature analysis of the WAG injectivity abnormalities in the CO_2 process. Improved oil recovery symposium, 3-5 April 2000, Tulsa, Oklahoma. SPE 59329. 5-16.

71. Sayegh, S.G., Krause, F.F., Girard, M., DeBree, C. (1990) Rock/Fluid Interactions of Carbonated Brines in a Sandstone Reservoir: Pembina Cardium, Alberta, Canada. SPE Formation Evaluation, December 1990, SPE 19392. 399-405.

72. Shah, V., Broseta, D., Mouronval, G. (2008) Capillary Alteration of Caprocks by Acid Gases, SPE 113353

73. Shahverdi, H., Sohrabi, M., Fatemi, M., Jamiolahmady, M., Irelan, S., Robertson, G. (2011) Evaluation of Three-Phase Relative Permeability Models for WAG Injection Using Water-Wet and Mixed-Wet Core Flood Experiments, SPE 143030

74. Shen, P., Zhu, B., Li, X.-B. (2006) The Influence of Interfacial Tension on Water/Oil Two-Phase Relative Permeability, SPE 95405

75. Skauge, A. (1994) Summary of core flood results in connection with WAG evaluation. Proceedings 10th Wyoming Enhanced Oil Recovery Symposium, University of Wyoming, Laramie, Wyoming.

76. Skauge, A. (1996) Influence of Wettability on Trapped Non-Wetting Phase Saturation in Three-Phase Flow. Proceedings 4th International Symposium on Wettability and it's Effect on Oil Recovery, Montpellier, France.

77. Skauge, A. and Aarra, M. (1993) Effect of wettability on the oil recovery by WAG. Proceedings 7th European Symposium on Improved Oil Recovery, Moscow.

78. Skauge, A. and Dale, E. I. (2007) Progress in Immiscible WAG modeling. SPE/EAGE Reservoir Characterization and Simulation Conference, Abu Dhabi, U.A.E. SPE 111435.

79. Skauge, A., Spildo, K., Høiland, L, Vik, B. (2006) Theoretical and experimental evidence of different wettability classes. Journal of Petroleum Science and Engineering 57 (2007), 321-333.

80. Skauge, A., Standal, S., Boe, S.O., Skauge, T., Blokhus, M. (1999) Effect of Organic Acids and Bases, and Oil Composition on Wettability, SPE 56673.

81. Skauge, A. and Stensen, J. Å (2003) Review of WAG field experience. Oil Recovery – 2003, 1st International Conference and Exhibition, Modern Challenges in Oil Recovery, Russia, Moscow, Gubkin University.

82. Skauge, A, and Larsen, J. A. (1994) Three-Phase Relative Permeability and Trapped Gas Measurements Related to WAG Processes, SCA-9421.

83. Skjæveland, S. M., Siqveland, L. M., Kjosavik, A., Hammervold Thomas, W. L. and Virnovsky, G. A. (2000) Capillary pressure correlation for mixed-wet reservoir, SPE Reservoir Evaluation and Engineering 3, pp 60-67

84. Sorbie, K.S., van Dijke, M.I.J. (2004) Fundamentals of three-phase flow in porous media of heterogeneous wettability. Institute of Petroleum Engineering, Heriot-Watt University, Edinburgh, Scotland, UK. 3-17.

85. Statoil/ Norsk Hydro/ Saga. (1984) Completion Report Well 31/6-2. Exploration and Production Division.

86. Statoil. (1984) Routine Core Analysis, Well 31/6-6. GECO, Geophysical Company of Norway A/S.

87. Steel, R.J., Felt, V.L., Johannessen, E.P., Mathieu, C. (1995) Sequence Stratigraphy on the Northwest European Margin. NPF, Special publication no. 5.

88. Stone, H. L. (1970) Probability model for estimating three-phase relative permeability, Trans AIME (JPT), 249, 214-218

89. Stone, H. L. (1973) Estimation of three-phase relative permeability and residual oil data, Canadian Petroleum Technology, Vol 12, 53-61.

90. Tamimi A., Rinker, E. B., Sandall, O.C. (1994) Diffusion coefficients for hydrogen sulfide, carbon dioxide, and nitrous oxide in water over the temperature range 293 – 368 K, J. Chem. Eng. Data

91. Todd, C.A., Tweedie, J. (1978) Total rock characterisation of north sea sandstones with particular reference to interstitial clays. European Offshore Petroleum Conference and Exhibition, London 24-27, 1978.

92. Tonnet, N., Shah, V., Chiquet, P., Diaz, J., Mouronval, G., Broseta, D. (2008) Wettability alteration of caprock minnerals by acid gases, 10th International Symposium on Reservoir Wettability, Abu Dhabi, 26-28 October 2008

93. Ülker, B., Alkan, H., Pusch, G. (2007) Implications of the Phase-Solubility Behaviour on the Performance Predictions of the CO_2 Trapping in Depleted Gas Reservoirs and Aquifers. SPE 107189. 1-8.

94. Valvatne, P. J., and Blunt, M. J., (2004) Predictive pore-scale modeling of two-phase flow in mixed-wet media, W07406, Water Resource Res., 40(7)

95. van Dijke, M. I. J., and Sorbie, K. S. (2002) Pore-scale network model for three-phase flow in mixed-wet porous media, Phys. Rev. E., 77, 046302

96. Virnovsky, G. A., Vatne, K.O., Iversen, J.E. (2004) Three-phase capillary pressure measurements in centrifuge at reservoir conditions, International Symposium of the Society of Core Analysts, Abu Dhabi, UAE

97. Vollset, J., Doré, A. G. (1984) A revised Triassic and Jurassic lithostratigraphic nomenclature for the Norwegian North Sea. NPD-Bulletin No. 3.

98. Wang, W., Gupta, A. (1995) Investigation of the Effect of Temperature and Pressure on Wettability using Modified Pendant Drop Method, SPE 30544

99. Wei. L.. Saaf. F. (2009) Estimate CO_2 storage capacity of the Johansen formation: numerical investigation beyond the benchmarking exercise. Springer Science 2009.

100. Yang, Y., Aplin, A.C. (2007) Permeability and petrophysical properties of 30 natural mudstones. Journal of Geophysical Research, VOL. 112, 2007.

101. Zolotukhin, A., Ursin, J. R. (2000) Introduction to petroleum reservoir engineering, Høyskoleforlaget, Kristiandsand.

102. Øren, P. E., Bakke, S., and Arntzen, O. J. (1998) Extending predictive capabilities to network models, SPEJ, 3(4), pp. 324-336

Nomenclature

A	cross section area
a_o	constant in the Corey type and Skjæveland et. al correlation
a_w	constant in the Corey type and Skjæveland et. al correlation
C	constant in the Corey correlation and Land correlation
c_o	constant in the Skjæveland et. al correlation
$C_{s,o}$	spreading coefficient
c_w	constant in the Skjæveland et. al correlation
dP	differential pressure
dx	differential distance
E	curvature parameter
E_o	constant in LET oil relative permeability correlation
E_w	constant in LET water relative permeability correlation
F	factor in Killough's correlation
F_{down}	downward force
F_{up}	upward force
g	gravity acceleration and conductance
h	height
k	permeability

$k_{eff,i}$	effective permeability for fluid i
k_{rg}	relative permeability for gas
k_{ri}	relative permeability for fluid i
k_{ro}	relative permeability for oil
k_{rog}	two-phase oil relative permeability in a gas-oil system
k_{row}	two-phase oil relative permeability in a oil-water system
k_{rw}	relative permeability for water
$(k_{rg})_{S_{orwg}}$	water relative permeability at residual oil saturation after gas injection
$(k_{ro})_{S_{gc}}$	oil relative permeability at critical gas saturation
$(k_{ro})_{S_{wi}}$	oil relative permeability at irreducible water saturation
$(k_{rw})_{S_{orwc}}$	water relative permeability at residual oil saturation after water injection
L_o	constant in LET oil relative permeability correlation
L_w	constant in LET water relative permeability correlation
n_g	gas relative permeability exponent
n_{og}	oil relative permeability exponent in presence of gas
n_{ow}	oil relative permeability exponent in presence of water
n_w	water relative permeability exponent
P_c	capillary pressure

$P_{c,aw}$	capillary pressure between air and water
P_{Cd}	drainage capillary pressure
$P_{C,entry}$	capillary entry pressure
P_{Cgo}	gas-oil capillary pressure
P_{Cgw}	gas-water capillary pressure
P_{Ci}	imbibition capillary pressure
P_{Cow}	oil-water capillary pressure
P_e	capillary entry pressure
$P_{entry,w}$	capillary entry pressure for water wet pores
$P_{non-wetting}$	pressure in non-wetting phase
P_{oil}	pressure in oil phase
P_{water}	pressure in water phase
$P_{wetting}$	pressure in wetting phase
q	flow rate
r	pore radius
$r_{\max}$	maximum pore radius
$r_{\min}$	minimum pore radius
S_e	effective saturation

S_g	gas saturation
S_g^*	effective gas saturation
S_{gc}	critical gas saturation
S_{gi}	initial gas saturation
S_{gt}	trapped gas saturation
S_{lc}	total critical liquid saturation
$S_{nw,\max}$	maximum saturation of the non-wetting fluid
$S_{nw,t}$	trapped saturation of the non-wetting fluid
S_o	oil. Saturation
S_o^*	effective oil saturation
S_{or}	residual oil saturation
S_{org}	residual oil saturation after gas injection
S_{orm}	minimum radius oil saturation
S_{orw}	residual oil saturation after water injection
S_w	water saturation
S_w^*	effective water saturation
$S_{w,hys}$	water saturation at hysteresis reversal point
S_{wi}	irreducible water saturation

S_{wir}	irreducible water saturation
S_{wn}	normalized water saturation
T_o	constant in LET oil relative permeability correlation
T_w	constant in LET water relative permeability correlation
V	volume
v	volume exponent
$x_{i\,\max}$	maximum value for parameter i
$x_{i\,\min}$	minimum value for parameter i
$x^0_{i\,\max}$	maximum value for parameter i from previous timestep
$x^0_{i\,\min}$	minimum value for parameter i from previous timestep
β_g	gas factor in the Stone I correlation
β_w	water factor in the Stone I correlation
$\Delta\rho$	difference in density
θ_a	advancing contact angle
θ_{aw}	angle between air-water interface and solid
θ_{go}	contact angle between gas-oil
θ_{gw}	contact angle between gas-water
θ_{ow}	contact angle between oil-water

θ_r	receeding contact angle
λ	pore size index and conductance exponent
μ_i	viscosity for fluid i
π	constant, approximately 3.14
ρ_a	density of air
ρ_w	density of water
σ	interfacial tension
σ_{aw}	interfacial tension between air and water
σ_{go}	interfacial tension between gas and oil
σ_{gs}	interfacial tension between gas and solid
σ_{gw}	interfacial tension between gas and water
σ_{os}	interfacial tension between oil and solid
σ_{ow}	interfacial tension between oil and water
σ_{ws}	interfacial tension between water and solid